A hybrid method for hydrodynamic-kinetic flow - Part I -A particle-gridmethod for reducing stochastic noise in kinetic regimes

A hybrid method for hydrodynamic-kinetic flow - Part I - A particle-grid method for reducing stochastic noise in kinetic regimes

Alessandro Alaia [*], Gabriella Puppo [*†]

November 25, 2010

Abstract

In this work we present a hybrid particle-grid Monte Carlo method for the Boltzmann equation, which is characterized by a significant reduction of the stochastic noise in the kinetic regime.

The hybrid method is based on a first order splitting in time to separate the transport from the relaxation step. The transport step is solved by a deterministic scheme, while a hybrid DSMC-based method is used to solve the collision step. Such a hybrid scheme is based on splitting the solution in a collisional and a non-collisional part at the beginning of the collision step, and the DSMC method is used to solve the relaxation step for the collisional part of the solution *only*. This is accomplished by sampling only the fraction of particles candidate for collisions from the collisional part of the solution, performing collisions as in a standard DSMC method, and then projecting the particles back onto a velocity grid to compute a piecewise constant reconstruction for the collisional part of the solution. The latter is added to a piecewise constant reconstruction of the non-collisional part of the solution, which in fact remains unchanged during the relaxation step.

Numerical results show that the stochastic noise is significantly reduced at large Knudsen numbers with respect to the standard DSMC method. Indeed in this algorithm, the particle scheme is applied only on the collisional part of the solution, so only this fraction of the solution is affected by stochastic fluctuations. But since the collisional part of the solution reduces as the Knudsen number increases, stochastic noise reduces as well at large Knudsen numbers.

Keywords: Numerical methods for kinetic flows, particle-grid method, Monte Carlo method.

AMS Subject classification: 65M75, 65C35, 76P05, 82C80

1 Introduction

Engineering problems frequently involve complex fluxes and geometries, and both kinetic and hydrodynamic regimes coexist in the same field of motion. In many engineering applications, in fact,

[*]Department of Mathematics, Politecnico di Torino, c.so Duca Degli Abruzzi 24, 10129, Torino, Italy. alessandro.alaia@polito.it, gabriella.puppo@polito.it

[†]Corresponding author.

the Knudsen number (defined as the ratio between the mean free path and the geometrical length scale) spans a wide range of values in the same computational domain, starting from very low values in hydrodynamic regions, to high values in kinetic ones.

In such cases, simulating the gas flow becomes a complex task because of the breakdown of continuum models in some regions of the physical domain. In hydrodynamic regions, where the Knudsen number reaches low values, the number of collisions per unit time (which is inversely proportional to the Knudsen number) is sufficiently large to make the velocity distribution close to the equilibrium distribution. Thus, macroscopic models such as Navier-Stokes or Euler equations, can be used to model the fluid flow, as the underlying assumption in such models is that the velocity distribution is close to the Maxwellian.

Conversely in kinetic regions, where the number of collisions per unit time is small, the velocity distribution can be very different from the equilibrium distribution. In such cases continuum models are not able to accurately describe the fluid behavior, and the Boltzmann equation must be used instead.

Two significant examples can be found, among others, in simulating the gas flow in MEMS devices where the Knudsen number is large because of the small geometrical length-scale of the device ([18]); or in simulating nozzle emissions in satellite control stability systems (C.S.S.), where the gas emitted by the nozzle expands in vacuum.

Of course, from a physical-mathematical point of view, one can use the Boltzmann equation to describe the flow field both in hydrodynamic and in kinetic regions, as it is well known that in the hydrodynamic limit (i.e. for a vanishing Knudsen number), both Euler and Navier-Stokes equations can be recovered from the Boltzmann equation via the Chapman-Enskog expansion, (see [9], [12]). However, from a practical point of view, this would require to solve the Boltzmann equation on the whole computational domain, using either deterministic or probabilistic methods.

Deterministic methods are characterized by a high computational demand, mainly due to the multidimensionality of the collisional integral.

Among stochastic numerical methods, the most successful category is represented by particle methods, and among these Direct Simulation Monte Carlo methods (see, [5], [25]) are by far the most used. However, some drawbacks inherent in DSMC methods limit their applicability. For instance, their computational efficiency strongly decreases in the hydrodynamic regime, so that DSMC methods are not suitable for simulating fluid flows at small Knudsen numbers. Moreover as a consequence of the probabilistic approach, numerical results are polluted by stochastic noise, which can be reduced using suitable time-space averages for steady problems, or averaging numerical results over multiple simulations for unsteady flows at the price of increasing the computational cost.

For all aforementioned reasons, an attractive idea is to design a *hybrid* scheme able to efficiently couple both macroscopic and kinetic models. Several schemes are available in the current literature, based on different strategies.

Some methods are based on the idea of numerically (or analytically) solving the kinetic model to provide additional information for the macroscopic model (see for instance [6]).

Another approach is based on solving both the kinetic and the hydrodynamic model on the whole computational domain, and the solution is recovered as a suitable average between the former and the latter. Typically, such a coupling is designed in order to automatically *switch* from the kinetic to the macroscopic model when the transition from kinetic to hydrodynamic regime occurs. For instance, in [14] and [15], the kinetic model is given by the BGK equation ([4]) and the solution is locally splitted in an equilibrium and a non-equilibrium part. The time evolution of the non-equilibrium part is evaluated by solving the BGK equation with a particle scheme, resulting in a significant reduction of the stochastic noise in hydrodynamic regimes where the non-equilibrium part of the solution - and thus stochastic fluctuations - reduces as the Knudsen number decreases.

Other methods are based on the idea of solving a *simplified* kinetic model on a finite set of

velocities, such that the desired macroscopic equations are recovered in the hydrodynamic limit. Among methods of this class, the Lattice Boltzmann Method (LBM) has successfully been used in several applications (see [29]).

Another possible approach is based on coupling the kinetic and the macroscopic models through a domain decomposition. For instance, in [28] the Boltzmann equation and Compressible Navier Stokes equations are coupled. The difficulty of coupling a deterministic and a stochastic solver are overcome because steady state solutions are sought, and thus the fluctuations of DSMC are damped through time averaging. Moreover the location of the kinetic and continuum regions is modified until steady state is reached. A similar approach can be found in [33], which also concentrates on steady state problems. On the other hand, Garcia et al. ([16]) compute unsteady solutions, but the domain decomposition is chosen at the initial time, so no indicator to drive the domain decomposition is needed. In their approach, an adaptive mesh refinement (AMR) algorithm is used. With the AMR approach, several DSMC cells are embedded in the larger cells where the continuum equations are solved, and if the need for cells of the same size of the mean free path arises, the Boltzmann equation is solved in these cells using a DSMC method. Then macroscopic quantities at the continuum level are evaluated averaging the DSMC solution over several space cells, thus damping stochastic fluctuations.

In [13], the domain decomposition is time dependent, but here two deterministic solvers interact, a finite volume scheme for the BGK equation at the kinetic level, and a finite volume scheme for the Compressible Euler equations. In [13] the domain decomposition is characterized by an overlapping between the kinetic and the hydrodynamic regions, that is a buffer region is considered at the interfaces between kinetic and hydrodynamic regions, where both the kinetic model and macroscopic equations are solved. Conversely in [7] the Boltzmann and the Navier-Stokes equations are coupled with a domain decomposition without overlapping. Finally in [31] a sophisticated equilibrium indicator is used to construct a time dependent domain decomposition, and two particle methods are coupled for the kinetic and for the continuum equations.

The main goal we would like to pursue in this work, is to efficiently couple the Boltzmann and Euler equations through a domain decomposition strategy.

We have in mind to start from the results in [31] and [32], constructing a time-dependent domain decomposition indicator based on the gradients of macroscopic quantities (specifically temperature and mean velocity), and on the local Knudsen number. Then starting from the domain decomposition, the Boltzmann and Euler equations will be coupled using the ES-BGK ([17], [2]) equation to provide a smooth transition between the kinetic and the macroscopic model. In order to take advantage of the low computational cost of particle methods, the Boltzmann equation will be solved with a DSMC-based method, while standard finite volume schemes will be used to integrate the ES-BGK (see [20], [21] and [27]) and Euler equations (see [19]). However, since the domain decomposition indicator will be based on the space gradient of some macroscopic quantities, a standard DSMC method will not be applicable in kinetic regions, as stochastic fluctuations inherent in the DSMC approach would ignite spurious gradients and produce an incorrect domain decomposition. Moreover, stochastic noise would also pollute numerical fluxes at the domain interfaces resulting in spurious oscillations in the continuum solution.

For these reasons, the present work is devoted to designing a hybrid particle-grid method able to reduce the stochastic noise in kinetic regimes. In Part II ([1]) we will use our hybrid scheme as the numerical solver for rarefied regimes, coupling the hybrid scheme with a finite volume solver for the ES-BGK and Euler equations.

The hybrid scheme presented in this paper, is based on the heuristic observation that in a space homogeneous problem solved with a standard DSMC scheme, no stochastic noise on macroscopic quantities is observed. On the contrary, if transport is included, stochastic fluctuations appear on macroscopic variables. The basic idea is thus to avoid particle advection as much as possible.

In order to do this, we propose to represent the velocity distribution as a piecewise constant function. At the beginning of the relaxation step the solution is splitted in a collisional and a non-collisional part. The former represents the velocity distribution of particles which are candidate for collision and can be interpreted as a velocity histogram.

Next, the velocity of candidate particles is sampled from the collisional part of the solution and collisions are performed as in a standard DSMC scheme. Candidate particles are then projected back onto a velocity grid in a conservative way to compute a piecewise constant reconstruction of the post-collisional distribution corresponding to candidate particles. This is added to the piecewise constant reconstruction of the non-collisional part, which in fact remains unchanged during the relaxation step. Finally, the transport step is deterministically solved for the whole solution.

In this fashion, only particles which are candidate for collisions are actually used during the relaxation step and they contribute to the stochastic noise on the collisional part of the solution only. But, since the number of candidate particles is inversely proportional to the Knudsen number, the collisional part of the solution decreases as the Knudsen number increases, so the stochastic noise reduces as well at large Knudsen numbers.

Conversely in hydrodynamic regimes, when the Knudsen number is small, the collisional part of the solution is dominant over the non-collisional part, the number of candidate particles is large and thus stochastic fluctuations have the same magnitude as in a standard DSMC method. However, this circumstance is never encountered as the domain decomposition in [1], allows for using the hybrid method only in kinetic regimes, where the local Knudsen number is large.

The remaining part of the present paper is organized as follows:

- In §2, we briefly recall the Boltzmann equation in order to fix the notation. For further details we refer the reader to [9], [10] and [11].
- In §3, we introduce some basic concepts about DSMC methods, and the framework used to derive the hybrid algorithm. More details on the topic can be found in [3] [5], [22], and [26].
- In §4, we derive the hybrid method.
- Lastly, in §5, we report some simple but meaningful tests to compare the hybrid algorithm with the standard DSMC method.

2 The Boltzmann equation

In this section we briefly recall some basic concepts about the Boltzmann equation. For a detailed description, we refer the reader to [5], [9], [10], and [11].

In this work we deal with the Boltzmann equation for a dilute monatomic gas, composed of molecules with mass m. Each molecule is characterized by position $\mathbf{x} \in \mathbb{R}^D$ and velocity $\mathbf{v} \in \mathbb{R}^d$, where $d \geq D$ is the total number of degrees of freedom of each molecule, and D is the number of dimensions in the physical space (for a monatomic gas typically $D = d = 3$, corresponding to molecules with 3 translational d.o.f., moving in a three dimensional space).

The Boltzmann equation describes the time evolution of the particle density distribution $f(\mathbf{x}, \mathbf{v}, t) : \mathbb{R}^D \times \mathbb{R}^d \times \mathbb{R} \to \mathbb{R}$, such that $f(\mathbf{x}, \mathbf{v}, t)\, d\mathbf{x}\, d\mathbf{v}$ is the mass of particles with position in $[\mathbf{x}, \mathbf{x} + d\mathbf{x}]$ and velocity ranging in $[\mathbf{v}, \mathbf{v} + d\mathbf{v}]$ at time t.

Under the assumptions:

(i) Position and velocity of each particle are uncorrelated;

(ii) Interaction between particles can be modeled as elastic impacts;

(iii) The probability of interaction between more than two particles is negligible;

(iv) No external forces act on particles;

(v) *Molecular chaos* (velocities of particles involved in a collision are uncorrelated);

the Boltzmann equation in dimensionless form reads as follows:

$$\begin{gathered} \partial_t f + \mathbf{v} \cdot \partial_{\mathbf{x}} f = Q\left(f,\, f\right) \\ Q\left(f,\, f\right) = \frac{1}{2\pi k n_\infty} \int_{\mathbb{R}^d} d\mathbf{v}_* \int_{S^{(d-1)}} d\mathbf{n}\, B\left(\left|\mathbf{v} - \mathbf{v}_*\right|, \mathbf{n}\right) \left[f'_* f' - f_* f\right] \end{gathered} \tag{1}$$

where $(\mathbf{v},\, \mathbf{v}_*)$ and $(\mathbf{v}', \mathbf{v}'_*)$, respectively represent the velocities of a test and a field particle before and after a collision, $\mathbf{n}$ is the impact direction, and $S^{(d-1)}$ is the surface of the unit sphere in the d-dimensional space. $B\left(\left|\mathbf{v} - \mathbf{v}_*\right|, \mathbf{n}\right)$ is called *impact parameter* and depends on the collision model. Lastly, f'_* is a shorthand for $f\left(\mathbf{x},\, \mathbf{v}'_*,\, t\right)$, and analogously for f', f_*.

kn_∞ is the Knudsen number in a reference condition that is the ratio between the mean-free path in the reference condition λ_∞ and the geometrical length-scale of the phenomenon. The mean free-path in reference conditions can be estimated as follows:

$$\lambda_\infty = \frac{m}{\sqrt{2}\pi\sigma^{d-1}\rho_\infty} \tag{2}$$

and ρ_∞ is a reference density value.

The l.h.s. of the Boltzmann equation describes the free-molecular motion, (i.e. particles are advected by their velocity),while the r.h.s is the so-called *collision integral* and provides the rate of change of the mass of particle in a control volume in the one particle phase space due to collision processes.

Elastic collisions preserve mass, momentum and energy; post-collisional velocities are thus given by:

$$\begin{aligned} \mathbf{v}' &= \mathbf{v} - \left[\left(\mathbf{v} - \mathbf{v}_*\right) \cdot \mathbf{n}\right] \mathbf{n} \\ \mathbf{v}'_* &= \mathbf{v}_* - \left[\left(\mathbf{v} - \mathbf{v}_*\right) \cdot \mathbf{n}\right] \mathbf{n} \end{aligned} \tag{3}$$

With simple calculations, it is possible to show that:

$$\left(\mathbf{v} - \mathbf{v}_*\right) \cdot \mathbf{n} = -\left(\mathbf{v}' - \mathbf{v}'_*\right) \cdot \mathbf{n} \tag{4}$$

$$\left|\mathbf{v} - \mathbf{v}_*\right| = \left|\mathbf{v}' - \mathbf{v}'_*\right| \tag{5}$$

The collision: $(\mathbf{v},\, \mathbf{v}_*) \rightarrow (\mathbf{v}',\, \mathbf{v}'_*)$ can also be interpreted as a change of variables, whose Jacobian is:

$$J\left(\mathbf{n}\right) = \begin{pmatrix} \mathbf{i} - \mathbf{n}\,\mathbf{n}^T & \mathbf{n}\,\mathbf{n}^T \\ \mathbf{n}\,\mathbf{n}^T & \mathbf{i} - \mathbf{n}\,\mathbf{n}^T \end{pmatrix} \tag{6}$$

and has a unit determinant. Here $\mathbf{i}$ denotes the identity matrix in $\mathbb{R}^d \times \mathbb{R}^d$.

In this work we consider the Hard Sphere model, in which molecules are modeled as rigid spheres with diameter σ. Collisions occur only if two molecules are in touch, so the impact direction is given by the normal vector on the spherical surface of the field particle at the contact point. The resulting impact parameter is given by:

$$B\left(\left|\mathbf{v} - \mathbf{v}_*\right|,\, \mathbf{n}\right) = \sigma^{d-1}\, \left|\left(\mathbf{v} - \mathbf{v}_*\right) \cdot \mathbf{n}\right| \tag{7}$$

Once the density distribution is known, macroscopic quantities, such as density, macroscopic velocity, temperature, can be computed as the moments of f. We have:

$$\begin{gathered}\rho(\mathbf{x},t)=\int d\mathbf{v}\, f(\mathbf{x},\mathbf{v},t), \quad \mathbf{u}(\mathbf{x},t)=\int d\mathbf{v}\,\mathbf{v}\, f(\mathbf{x},\mathbf{v},t), \quad E(\mathbf{x},t)=\int d\mathbf{v}\,\frac{1}{2}|\mathbf{v}|^2 f(\mathbf{x},\mathbf{v},t) \\ \mathbf{q}(\mathbf{x},t)=\int d\mathbf{v}\,\frac{1}{2}\mathbf{v}|\mathbf{v}-\mathbf{u}|^2 f(\mathbf{x},\mathbf{v},t), \quad \boldsymbol{\tau}=\int d\mathbf{v}\,(\mathbf{v}-\mathbf{u})\otimes(\mathbf{v}-\mathbf{u})(\mathbf{x},\mathbf{v},t)\end{gathered} \tag{8}$$

where ρ is the macroscopic density, $\mathbf{u}$ is the macroscopic velocity, E is the total energy linked to the temperature by the following relationship: $E=\frac{d}{2}\rho\mathcal{R}T+\frac{1}{2}\rho|\mathbf{u}|^2$, $\mathbf{q}$ is the heat flux, and $\boldsymbol{\tau}$ is the pressure tensor whose trace is linked to the pressure by the relationship: $p:=\frac{1}{d}tr(\boldsymbol{\tau})=\rho\mathcal{R}T$. Here $\mathcal{R}$ represents the gas constant which is the ratio between the universal gas constant and the gas molar mass.

The time evolution of f is the result of the competition between collisional processes (by means of which the system tries to reach the local equilibrium), and advection which destroys the structure of the equilibrium. The equilibrium distribution is the Maxwellian univocally defined by macroscopic quantities:

$$\mathcal{M}_f[\rho,\mathbf{u},T]=\frac{\rho}{(2\pi\mathcal{R}T)^{d/2}}\exp\left(-\frac{|\mathbf{v}-\mathbf{u}|^2}{2\mathcal{R}T}\right) \tag{9}$$

It is possible to prove that the Maxwellian distribution minimizes the $\mathcal{H}$-functional defined by $\mathcal{H}=\int d\mathbf{v} f\log f$, and is the only distribution in the kernel of the collision operator.

3 The DSMC method

In this section we will briefly recall the DSMC method on which the hybrid algorithm is based. More details can be found in [3] [5], [22], [26] and [24].

For simplicity, let us consider the one-dimensional problem:

$$\begin{cases}\partial_t f+v\cdot\partial_x f=\dfrac{1}{2\pi k n_\infty}Q(f,f), \quad x\in[a,b],\,\mathbf{v}\in\mathbb{R}^d,\,t\in\mathbb{R}_+\\ f(x,\mathbf{v},t=0)=f_0(\mathbf{v})\\ +\text{boundary conditions}\end{cases} \tag{10}$$

The key idea of the DSMC method is to approximate the evolution of the system described by the Boltzmann equation with the evolution of a statistical sample of N particles, each of them with mass μ, position $\chi_j(t)$ and velocity $\xi_j(t)$, $j=1,\ldots,N$.

Particles' positions and velocities are updated according to the dynamic described by the Boltzmann equation, so that once the position and the velocity of each particle are known at time t the density distribution f is given by:

$$f(x,\mathbf{v},t)=\mu\sum_{j=1}^{N}\delta(x-\chi_j(t))\,\delta(\mathbf{v}-\xi(t)). \tag{11}$$

If the physical domain is discretized in N_x cells, the cell averages of macroscopic quantities can be computed starting from (11) as follows:

$$
\begin{aligned}
(\rho,\, \rho\mathbf{u},\, E)_i^T(t) &= \frac{\mu}{\Delta x_i} \int_{C_i} dx \int_{\mathbb{R}^d} d\mathbf{v} \sum_{j=1}^{N} \phi(\mathbf{v})\, \delta(x - \chi_j(t))\, \delta(\mathbf{v} - \xi_j(t)) \\
&= \frac{\mu}{\Delta x_i} \sum_{j \in \mathcal{I}_i(t)} \phi(\xi_j)
\end{aligned}
\tag{12}
$$

where $\phi(\mathbf{v}) := \left(1,\, \mathbf{v},\, \frac{1}{2}|\mathbf{v}|^2\right)^T \in \mathbb{R}^{d+2}$ is the moments vector, C_i is the i-th cell with volume Δx_i, $i = 1, \ldots, N_x$, and $\mathcal{I}_i$ is the collection of indices of particles with position in C_i, i.e $\mathcal{I}_i := \{j \in \{1, \ldots, N\} : \chi_j(t) \in C_j\}$.

If we introduce a discretization of the velocity space as well, the space-velocity cell averages of f can be computed by integrating (11) over $C_i \times V_{\mathbf{k}}$:

$$
\begin{aligned}
f_{i,\mathbf{k}}(t) &= \frac{\mu}{\Delta\mathbf{v}\Delta x} \int_{C_j} dx \int_{V_{\mathbf{k}}} d\mathbf{v} \sum_{j=1}^{N} \delta(x - \chi_j(t))\, \delta(\mathbf{v} - \xi_j(t)) \\
&= \frac{\mu}{\Delta x \Delta\mathbf{v}} \sum_{j \in \mathcal{I}_{i,\mathbf{k}}(t)} 1
\end{aligned}
\tag{13}
$$

Here $V_{\mathbf{k}}$ is the $\mathbf{k}$-th cell in the velocity cell with volume $\Delta\mathbf{v}_{\mathbf{k}}$, and
$\mathcal{I}_{i,\mathbf{k}}(t) := \{j \in \{1, \ldots, N\} : \chi_j(t) \in C_i \wedge \xi_j(t) \in V_{\mathbf{k}}\}$.

Note that (13) can be interpreted both as a piecewise constant reconstruction of f, and as a histogram reporting the absolute frequency of particles in the space-velocity cell $C_i \times V_{\mathbf{k}}$ multiplied by the ratio $\mu/\Delta x_i \Delta\mathbf{v}_{\mathbf{k}}$.

3.1 First order time splitting

The first step in the construction of the DSMC method is a time splitting to separate the relaxation from the transport step over a time interval Δt, that is we decouple collision processes and molecular movements over Δt with a first order accuracy in time.

The relaxation step is given by:

$$
\mathcal{R}_{\Delta t} : \begin{cases} \partial_t f^{(R)} = \dfrac{1}{2\pi k n_\infty} Q\left(f^{(R)},\, f^{(R)}\right), \quad x \in [a,b],\, \mathbf{v} \in \mathbb{R}^d,\, t \in [0, \Delta t] \\ f^{(R)}(x, \mathbf{v}, t = 0) = f(x, \mathbf{v}, t) \end{cases}
\tag{14}
$$

The transport step reads as follows:

$$
\mathcal{T}_{\Delta t} : \begin{cases} \partial_t f^{(T)} + \xi \cdot \partial_x f^{(T)} = 0, \quad x \in [a,b],\, \mathbf{v} \in \mathbb{R}^d,\, t \in [0, \Delta t] \\ f^{(T)}(x, \mathbf{v}, t = 0) = f^{(R)}(x, \mathbf{v}, \Delta t) \end{cases}
\tag{15}
$$

Solution at time $t + \Delta t$ can be approximated as $f(x, \mathbf{v}, t + \Delta t) = \mathcal{T}_{\Delta t}\, \mathcal{R}_{\Delta t} f(x, \mathbf{v}, t)$, which means that at first particle velocities are modified by collisions (relaxation step) but their positions remain unchanged, then particle positions change (transport step) but their velocities do not.

Therefore, the typical DSMC procedure is articulated in three steps:

1. A set of N particles is generated at the initial time with velocity distributed according to the initial data $f_0(x, \mathbf{v})$, and with number density proportional to the macroscopic density profile $\rho_0(x)$;

2. At each time step the velocities of particles are modified during the relaxation step, while their positions remain unchanged;

3. Then the positions of particles are modified during the transport step, but their velocities remain unchanged.

3.2 DSMC relaxation step

In order to solve the relaxation step by means of a particle method, one needs to estimate the number of collisions occurring during the time interval Δt. For this purpose, an upper bound (Σ) for the impact parameter is introduced, such that:

$$\Sigma = \max_{i,j} |\xi_i - \xi_j| \tag{16}$$

Then the 'modified' impact parameter, B_Σ, is defined as follows:

$$B_\Sigma \left(|\mathbf{v} - \mathbf{v}_*| , \mathbf{n} \right) = \min \left\{ B \left(|\mathbf{v} - \mathbf{v}_*| , \mathbf{n} \right) , \Sigma \right\} \tag{17}$$

Note that, thanks to the particular choice of Σ, for any pair of particles, one has:

$$B_{\Sigma i,j} := B_\Sigma \left(|\xi_i - \xi_j| , \mathbf{n} \right) \equiv B_{i,j} \qquad \forall i, j = 1, \ldots, N$$

where $B_{i,j} = B \left(|\xi_i - \xi_j| , \mathbf{n} \right)$.

By the previous property, and since in DSMC methods the collision integral is evaluated only on particles velocities, one can replace B with B_Σ without introducing any arbitrariness. Then, using an explicit first order time integration method, the relaxation step can be rewritten as follows:

$$\begin{aligned} Q \left(f, f \right) &= \frac{2\Sigma\rho}{k n_\infty} P \left(f, f \right) + \frac{2\Sigma\rho}{k n_\infty} f \\ P \left(f, f \right) &= \frac{1}{4\pi\rho} \left[\int_{S^2} d\mathbf{n} \int_{\mathbb{R}^d} d\mathbf{v}_* \frac{B_\Sigma}{\Sigma} f' \, f'_* + \int_{S^2} d\mathbf{n} \int_{\mathbb{R}^d} d\mathbf{v}_* \frac{\Sigma - B_\Sigma}{\Sigma} f \, f_* \right] \end{aligned} \tag{18}$$

where the superscript '(R)' has been omitted to simplify the notation.

If a first order explicit time integration method is used, the relaxation step becomes:

$$\begin{aligned} f^{n+1} &= p^n \, P \left(f^n, f^n \right) + (1 - p^n) f^n \\ p^n &= \frac{2\rho^n \Sigma \Delta t}{k n_\infty} \end{aligned} \tag{19}$$

If the time step is such that:

$$0 \leq \Delta t \leq \frac{k n_\infty}{2\rho^n \Sigma} \quad \Rightarrow \quad 0 \leq p^n \leq 1 \tag{20}$$

thus p^n can be interpreted as an estimate (in excess) of the probability that a particle will collide during the time interval Δt. So, the r.h.s. of (19) becomes a convex combination of density distributions with the following probabilistic interpretation. The first term on the r.h.s. of (19) can be interpreted as the velocity distribution of particles which certainly do *not* collide during Δt. Thus, the velocity distribution of such particles is unchanged within the relaxation step. Conversely, the second term on the r.h.s. of (19) can be interpreted as the post-collisional distribution of the remaining particles, to which we will refer as *candidates for collisions* (in short *candidates*). Each of them actually collides with probability B_Σ / Σ, so the post-collisional distribution of candidate particles, $\mathcal{P} \left(f^n, f^n \right)$, is composed of two terms:

- the first term represents the velocity distribution of candidate particles which really collide during Δt;

- the second term represents the post-collisional distribution of candidate particles which do not really collide within the relaxation step and whose velocity distribution does not change within the relaxation step.

Following the probabilistic interpretation of (19), the number of pairs of candidates in the space cell C_i is given by:

$$N_{c_i}^{\ n} = \left\lceil \frac{1}{2} p_i^n \frac{\rho_i^n \Delta x_i}{\mu} \right\rceil \tag{21}$$

where $\lceil x \rfloor$ is a probabilistic rounding of the real x.

If $\Delta x_i \approx \lambda$, the $N_{c_i}^{\ n}$ candidate pairs can be built choosing at random $2N_{c_i}^{\ n}$ particles among the N_i^n particles within the same space cell C_i. If further $\Delta t \approx \tau$, each particle collides only once during the time step, so in order to ensure that each particle takes part in only one collision, the sampling must be performed *without replacement*.

However, since the collision probability is over-estimated, the number of candidates is actually greater than the number of colliding particles. Thus, if all candidate pairs collided, a wrong number of collisions would be performed resulting in a faster relaxation toward the local equilibrium.

For this reason, colliding pairs are chosen among candidate pairs using an *acceptance-rejection* algorithm. This is accomplished for each candidate pair by choosing at random the impact direction uniformly from the unit sphere, and computing the modified impact parameter $B_{\Sigma j} = B_\Sigma \left(\left| \xi_j - \xi_{*j} \right|, \mathbf{n}_j \right)$, where $\mathbf{n}_j$ is the impact direction for the j-th couple, $j = 1, \ldots, N_{c_i}^{\ n}$. Then the j-th candidate pair is *accepted* as a colliding pair only if $B_{\Sigma j}, /\Sigma > \varepsilon_j$ (here ε_j is a random number sampled from a uniform distribution over $[0, 1]$). In this case, post-collisional velocities are computed according to the collisional model (3).

On the contrary, if $B_{\Sigma j}/\Sigma \leq \varepsilon_j$, the candidate pair is said to be *rejected* and particle velocities remain unchanged.

The resulting algorithm is the Nanbu-Babowski method [22] and it is summarized at the end of the present section.

Since collisions are local, positions of all particles are unchanged within the relaxation step, so the set of particles at the end of the relaxation step is given by $\left(\chi_j^n, \xi_j^{n+1} \right)$, $j = 1, \ldots, N$, and f is given by:

$$f^{(R)}\left(x, \mathbf{v}, \Delta t\right) = \mu \sum_{j=1}^{N} \delta\left(x - \chi_j^n\right) \, \delta\left(\mathbf{v} - \xi_j^{n+1}\right) \tag{22}$$

where ξ_j^{n+1} is the velocity of the j-th particle after the relaxation step.

Algorithm 3.1 ***Nanbu Babowski*** *- Relaxation step*
At each time step, for $i = 1, \ldots, N_x$

- *Compute the number of pairs candidate for collisions:* $N_{ci}^{\,n}$*;*
- *Choose at random* $2N_{ci}^{\,n}$ *particles without replacement among particles within the same space cell* C_i*;*
- *Build the* $N_{ci}^{\,n}$ *pairs candidate for collisions:* $\left(\xi_j^n,\, \xi_{*j}^{\,n}\right)$
- *for* $j = 1, \ldots, N_{ci}^{\,n}$
  - *Sample the impact direction uniformly from the unit sphere:* $\boldsymbol{n}_j$*;*
  - *Compute the modified impact parameter:* $B_{\Sigma j}$
  - *if* $B_{\Sigma j}/\Sigma > \varepsilon_j$
    - *Compute post-collisional velocities:* $\xi_j^{n+1} = \xi_j'$, $\xi_{*j}^{\,n+1} = \xi_*'$*;*
  - *else*
    - $\xi_j^{n+1} = \xi_j^n$, $\xi_{*j}^{\,n+1} = \xi_{*j}^{\,n}$*;*
  - *end*
- *end*

end.

3.3 DSMC transport step

After collisions are performed, the transport step is solved using (15) as initial data. The exact solution of the transport step is:

$$f^{(T)}\left(x, \mathbf{v}, \Delta t\right) = \mu \sum_{j=1}^{N} \delta\left(x - \chi_j^{n+1}\right)\, \delta\left(\mathbf{v} - \xi_j^{n+1}\right) \tag{23}$$

where:

$$\chi_j^{n+1} = \chi_j^n + \Delta t\, \xi_j^{n+1} \tag{24}$$

Since we assumed $\Delta x_i \approx \lambda \quad \forall i = 1, \ldots, N_x$ and $\Delta t \approx \tau$, each particle cannot cover a distance greater than the cell spacing, so the following restriction on the time step must be imposed:

$$\Delta t \leq \frac{\min\limits_{i=1,\ldots,N_x} \Delta x_i}{\max\limits_{j=1,\ldots,N} \left|\xi_j^{n+1}\right|} \tag{25}$$

This condition, which is similar to the CFL condition, can be estimated choosing a numerical value for the constant C, such that the probability of finding a particle with velocity $|\xi| > |u_i^n| + C\sqrt{T_i^n}$ is negligibly small. Note, however, that $\sqrt{T_i^n}$ is used instead of the sound speed and $C > 1$. In this case, in fact, one must consider also particles which travel faster then the thermal velocity, so (25) is more restrictive than the CFL condition used in numerical methods for macroscopic equations.

Boundary conditions are also considered during the transport step, deleting particles which leave the physical domain, and generating new particles according to the velocity distribution at boundaries.

Remark 3.2 *Note that no reconstruction of f is needed to advance the scheme in time, but we only need to compute ρ_i^n, and to store the indices of particles hosted in each space cell at each time step.*

Remark 3.3 *The computational efficiency of DSMC algorithms deteriorates when the fluid approaches the hydrodynamic regime. In this case the mean free path becomes small and both the time step (which is directly proportional to the Knudsen number), and the grid spacing (which is of the same order than the mean free path) become small.*

Remark 3.4 *The estimate of the upper bound in eq.* (16) *requires N^2 operations (where N is typically in the order of 10^4 or greater). We can simplify the estimate of Σ using the same device as in* (25)*, so that Σ is simply given by $\Sigma \geq 2C \max_{i=1,\ldots,N_x} \sqrt{T_i^0}$.*

Such an estimate is based on the initial temperature profile T_i^0, so it should be updated at each time step. However the only changes in the numerical value of Σ are due to the introduction of new particles in the computational domain. Indeed if we neglect the contribution of such particles, with the above choice of Σ we have that: $\left|\xi_i^0 - \xi_j^0\right| \leq \Sigma$, $\forall i, j$, but since the property in (4)*, we also have that $\left|\xi_i^n - \xi_j^n\right| \leq \Sigma$, $\forall i, j, n$.*

So, if the numerical value of C is properly set at the initial time the estimate of Σ remains valid at each subsequent time step, unless new particles are introduced in the computational domain. If this is the case the numerical value Σ can be updated during the relaxation step by setting $\Sigma = \max\left\{\Sigma, B_{\Sigma j}\right\}$ after each accepted collision, $j = 1, \ldots, N_{c_i}^{\ n}$.

3.4 Stochastic noise in DSMC simulations

As a consequence of the probabilistic approach, results provided by DSMC methods are polluted by stochastic noise, which is generated during both the relaxation and the transport step.

In order to highlight the difference between the stochastic noise generated during the relaxation step and the stochastic noise generated during the transport step, we consider a one dimensional problem with periodic boundary conditions, and $d = 2$ (particles with two translational degrees of freedom).

The physical domain is the interval [0, 1], and the initial data is (dimensionless variables):

$$f_0(x, \mathbf{v}) = \frac{\rho_1}{(2\pi T_1)^{d/2}} \exp\left(-\frac{|\mathbf{v} - \mathbf{u}_1|^2}{2T_1}\right) + \frac{\rho_2}{(2\pi T_2)^{d/2}} \exp\left(-\frac{|\mathbf{v} - \mathbf{u}_2|^2}{2T_2}\right) \tag{26}$$

$$\rho_1 = 1/2, \quad \mathbf{u}_1 = (2,\, 0)^T, \quad T_1 = 1$$
$$\rho_2 = 1/2, \quad \mathbf{u}_2 = (-2,\, 0)^T, \quad T_2 = 1$$

The time evolution of f is simply an asymptotic relaxation toward the local equilibrium, so the exact solution (for time approaching to infinity) is the Maxwellian distribution defined by the following macroscopic quantities:

$$\rho = 1, \quad \mathbf{u} = (0,\, 0)^T, \quad T = 3.$$

Since the initial data does not depend on the space coordinate, we can solve the following space-homogeneous problem as well:

$$\begin{cases} \dfrac{\partial f}{\partial t} = \dfrac{1}{2\pi k n_\infty} Q(f,\, f), \quad x \in [0,1] \\ f(x, \mathbf{v}, t = 0) = f_0(x, \mathbf{v}) \end{cases} \tag{27}$$

with the initial data given again by (26).

If the DSMC method described in this section is used for the full problem, one must solve both the relaxation step and the transport step using the particle scheme, while the space homogeneous problem requires that only the relaxation step is solved in each space cell at each time step.

Numerical results are reported in fig. 1 for a single simulation run with $kn_\infty = 10^{-2}$, $N_x = 200$, $\mu = 2.5 \cdot 10^{-5}$ (corresponding to 200 particles in each space cell) for both the full and the space homogeneous problem. In both cases, also a uniform discretization of the bounded velocity space $\mathbb{V} := [-10, 10] \times [-10, 10]$ with 50 cells on each direction of the velocity space was introduced to evaluate the velocity histogram at time $t = 0.2$ in $x = 0.5$.

Numerical results show that in both cases velocity histograms are affected by stochastic fluctuations (see fig. 1.a). However, since no particles are advected in the space homogeneous problem, the stochastic noise averages out from macroscopic profiles. On the contrary significant fluctuations are present on macroscopic quantities if also the transport step is solved by the particle scheme (see fig. 1.b).

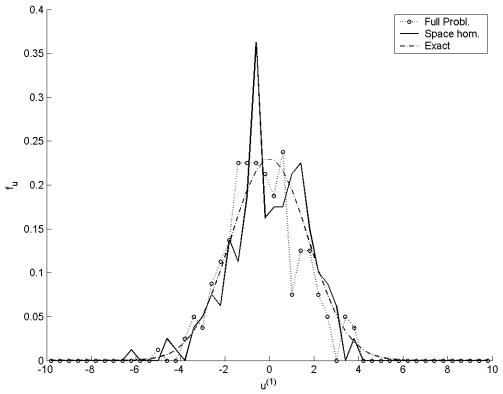

(a) Velocity distribution with respect to the first component of the microscopic velocity in $x = 0.5$ at $t = 0.2$

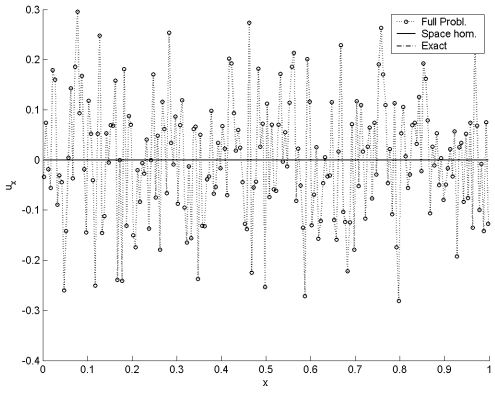

(b) Macroscopic x-velocity at $t = 0.2$

Figure 1: Numerical results for the full problem (circles), for the space homogeneous problem (continuous line) and exact solution (dashed line)

4 The Hybrid method

Numerical results presented in the previous section, show that the stochastic noise on macroscopic quantities is amplified during particle advection. In order to avoid such a phenomenon, one should solve the transport step using a deterministic scheme instead of advecting particles.

An interesting possibility is thus to design a *hybrid* particle-grid method which uses a deterministic scheme to solve the transport step and a DSMC method to solve the relaxation step.

Such a hybrid scheme would be articulated as follows:

- at the beginning of the relaxation step, a set of candidate particles is sampled from the solution;
- the relaxation step is solved using the DSMC method for candidate particles only;

- particles are projected onto a velocity grid at the end of the relaxation step to compute a reconstruction of the solution;
- the transport step is solved by a deterministic scheme using the reconstruction computed in the previous point as initial data.

The main drawback of such an algorithm is the computational cost due to particle sampling and projection. However, since in the DSMC method only candidate particles contribute to collisional processes, we can avoid to sample the whole particle set, but we can generate only the fraction of candidate particles at each time step.

This corresponds to splitting the solution in a collisional and a non-collisional part. The collisional part represents the velocity distribution of particles which are candidate for collisions, while the non-collisional part represents the velocity distribution of particles which are not candidate for collisions. The DSMC scheme is then used to evaluate the post-collisional distribution corresponding to the collisional part only.

The main advantage of such a scheme is that only the collisional part of the solution is affected by stochastic fluctuations. But since the number of candidate particles is inversely proportional to the Knudsen number, the collisional part of the solution reduces as the Knudsen number increases. Consequently, also the magnitude of stochastic fluctuations reduces at large Knudsen numbers.

In the next subsection we will build the scheme outlined above, starting from the Nanbu-Babowski algorithm presented in §3.

Note that a similar approach can be found in [15], where however the BGK model is considered instead of the Boltzmann equation. The hybrid scheme proposed in [15] is based on the idea of splitting the solution in an equilibrium and a non-equilibrium part. A particle scheme is used to solve both the relaxation and the transport step for the non-equilibrium part only, while the streaming step for the equilibrium part is solved by a deterministic scheme. The resulting algorithm allows to reduce stochastic fluctuations on macroscopic quantities in the limit of vanishing Knudsen numbers, when the equilibrium part of the solution is preponderant with respect to the non-equilibrium part.

The splitting proposed by Dimarco and Pareschi exploits the fact that in the standard BGK model the relaxation time only depends on macroscopic quantities. So, if an explicit time integration method is used, one can estimate *a priori* the fraction of solution which will relax toward equilibrium at the beginning of each time step. On the contrary, in the Boltzmann equation the collision rate depends on the microscopic velocity through the impact parameter, so the approach proposed in [15] cannot be extended in a trivial manner to the present case.

4.1 Hybrid method - Relaxation step

The relaxation step for the hybrid algorithm will be obtained in three steps:

(i) First, we will introduce the collisional splitting discussed in the beginning of the present section and we will rewrite the DSMC relaxation step in terms of the collisional part of the solution;

(ii) Second, we will introduce the particle approximation for the collisional part of the solution;

(iii) We will obtain a recipe to update the cell averages of the solution at the end of the relaxation step

Following the idea of splitting the solution in a collision and a non collisional part, let us introduce f_c and f_{nc}, which respectively represent the velocity distribution of particles which are candidate for collisions, and the velocity distribution of particles which are not candidate for collisions. Since the probability of a particle to be chosen as a candidate for a collision is independent from its velocity, we can define f_c and f_{nc} as follows (*collisional splitting*):

$$
\begin{aligned}
f &= f_c + f_{nc} \\
f_c = p\, f, \quad & f_{nc} = f - f_c = (1-p)\ f
\end{aligned}
\tag{28}
$$

At this point, we can rewrite the DSMC relaxation step in terms of f and f_c only. Using the definition of f_c the product $p\,\mathcal{P}\left(f,\, f\right)$ can be rewritten as:

$$
\begin{aligned}
p\,\mathcal{P}\left(f,\, f\right) = \frac{1}{4\pi\rho_c}\Bigg[& \int_{\mathcal{S}^{d-1}} d\mathbf{n} \int_{\mathbb{R}^d} d\mathbf{v}_* \frac{B_\Sigma}{\Sigma} \frac{1}{\rho_c} {f_c}'_* \, {f_c}' + \\
& \int_{\mathcal{S}^{d-1}} d\mathbf{n} \int_{\mathbb{R}^d} d\mathbf{v}_* \frac{\Sigma - B_\Sigma}{\Sigma} f_{c*}\, f_c \Bigg] = \mathcal{P}\left(f_c,\, f_c\right)
\end{aligned}
\tag{29}
$$

where $\rho_c := p\,\rho$ is the mass fraction of particles candidate for collisions and the superscript $^{(R)}$ has been omitted for simplicity.

Thus the DSMC relaxation step becomes:

$$
{f}^{n+1} = {f_{nc}}^n + \mathcal{P}\left({f_c}^n,\, {f_c}^n\right) \tag{30}
$$

Eq. (30) shows that collisional processes only affect the collisional part of the solution, while the non-collisional part remains frozen during the relaxation step.

In order to take advantage of the low computational cost of particle methods, we employ the Monte Carlo method to approximate the collisional part of the solution only.

Thus at the beginning of the relaxation step, we need to 'convert' f_c into particles, i.e. we need to generate a sample of particles whose velocity is distributed according to f_c, and whose total mass is ρ_c. Equivalently, since the velocity distribution of candidate particles is the same as f except for a multiplicative factor which is independent from $\mathbf{v}$, we can sample a mass ρ_c of particles from f.

Let us suppose, that such a sample of particles is available, that the number of particles is N and that the j-th particle has velocity ξ_j and mass μ_j.

Since during the relaxation step particle positions are not modified, and since the particle set will be discarded at the end of the relaxation step, the x dependence is momentarily dropped.

Lastly note that while in the standard DSMC method all particles have the same mass, here we assumed that particle masses can be different. The reasons of this particular choice will be explained in section §4.3.

Given the particle set, we approximate ${f_c}^n$ as follows:

$$
{f_c}^n = \sum_{j=1}^{N} \mu_j\, \delta\left(\mathbf{v} - \xi_j^n\right) \tag{31}
$$

Consequently the product $f_c\left(\mathbf{v}\right)\ f_c\left(\mathbf{v}_*\right)$ appearing in the operator $\mathcal{P}$ becomes:

$$
\begin{aligned}
{f_c}^n\left(\mathbf{v}\right)\ {f_c}^n\left(\mathbf{v}_*\right) &= \sum_{j=1}^{N}\sum_{i=1}^{N} \mu_j\mu_i\, \delta\left(\mathbf{v} - \xi_j^n\right)\ \delta\left(\mathbf{v}_* - \xi_i^n\right) \\
&= \sum_{j=1}^{N} \mu_j^2\, \delta\left(\mathbf{v} - \xi_j^n\right)\ \delta\left(\mathbf{v}_* - \xi_j^n\right) \\
&+ \sum_{j=1}^{N}\sum_{i=j+1}^{N} \mu_j\mu_i\, \delta\left(\mathbf{v} - \xi_j^n\right)\ \delta\left(\mathbf{v}_* - \xi_i^n\right) \\
&+ \sum_{j=1}^{N}\sum_{i=j+1}^{N} \mu_j\mu_i\, \delta\left(\mathbf{v} - \xi_i^n\right)\ \delta\left(\mathbf{v}_* - \xi_j^n\right)
\end{aligned}
\tag{32}
$$

where in the second equality we used the symmetry with respect to the indices i and j.

Once all the possible $N(N-1)/2$ pairs are built and the index k running over pairs is defined, eq. (32) can be rewritten as follows:

$$\begin{aligned} {f_c}^n(\mathbf{v})\ {f_c}^n(\mathbf{v}_*) = &\sum_{j=1}^{N} \mu_j^2\, \delta\left(\mathbf{v}-\xi_j^n\right)\ \delta\left(\mathbf{v}_*-\xi_j^n\right) \\ &+ \sum_{k=1}^{N(N-1)/2} \hat{\mu}_k \delta\left(\mathbf{v}-\xi_k^n\right)\ \delta\left(\mathbf{v}_*-{\xi_*}_k^n\right) \\ &+ \sum_{k=1}^{N(N-1)/2} \hat{\mu}_k \delta\left(\mathbf{v}-{\xi_*}_k^n\right)\ \delta\left(\mathbf{v}_*-\xi_k^n\right) \end{aligned} \tag{33}$$

where $k = k(i,j)$ is the index of the couple $\left(\xi_j^n,\, \xi_i^n\right)$ and $\hat{\mu}_k = \mu_i\, \mu_j$.

At this point, it is straightforward to note that when particles are indexed by pairs, both particles in the same couple $(\xi_k^n,\, {\xi_*}_k^n)$ have the same mass $\hat{\mu}_k$; thus the collision $(\xi_k^n, {\xi_*}_k^n)$ involves particles with equal masses.

However, the value of $\hat{\mu}_k$ is different for each pair, but this is not at variance with the Boltzmann equation as $\hat{\mu}_k$ cannot be interpreted as a physical parameter, but must be interpreted as a weighting factor which expresses the contribution of the k-th collision on ${f_c}_{\mathbf{k}}^{n+1}$ relatively to the whole mass fraction ρ_c^n of candidate particles.

The final goal of the hybrid relaxation step is to provide a reconstruction of the solution, which will be used as initial data to deterministically solve the transport step. Since the DSMC method is only first order accurate in both space and time, we choose a piecewise constant reconstruction which is enough to preserve the order of accuracy. We can now compute the cell averages of f^{n+1} from (30). We get:

$$f_{\mathbf{k}}^{n+1} = f_{\mathbf{k}}^n - \frac{1}{\Delta v_{\mathbf{k}}} \int_{V_{\mathbf{k}}} {f_c}^n d\mathbf{v} + \frac{1}{\Delta v_{\mathbf{k}}} \int_{V_{\mathbf{k}}} \mathcal{P}\left({f_c}^n,\, {f_c}^n\right) \tag{34}$$

The second term on the r.h.s. of eq. (34) gives the following contribution:

$$\begin{aligned} \int_{V_{\mathbf{k}}} {f_c}^n d\mathbf{v} &= \sum_{j=1}^{N} \mu_j \int_{V_{\mathbf{k}}} \delta\left(\mathbf{v}-\xi_j^n\right) d\mathbf{v} \\ &= \sum_{j=1}^{N} \mu_j \mathbb{1}_{\xi_j^n \in V_{\mathbf{k}}} \end{aligned} \tag{35}$$

where the indicator function $\mathbb{1}_{\xi \in V_{\mathbf{k}}}$ is defined as:

$$\mathbb{1}_{\xi \in V_{\mathbf{k}}} := \begin{cases} 1, & \text{if} \quad \xi \in V_{\mathbf{k}} \\ 0, & \text{otherwise} \end{cases}$$

Then, we rewrite the third term on the r.h.s. of eq. (30) as follows:

$$\int_{V_{\mathbf{k}}} \mathcal{P}\left({f_c}^n,\, {f_c}^n\right) d\mathbf{v} = \frac{1}{4\pi\rho_c} \int_{\mathcal{S}^{d-1}} d\mathbf{n}\left[A_1 + A_2 + A_3 + B_1 + B_2 + B_3\right] \tag{36}$$

where the terms A_i, B_i, $i = 1, 2, 3$, are defined and computed below.

The term A_1 gives:

$$\begin{aligned} A_1 &= \int_{V_{\mathbf{k}}} d\mathbf{v} \int_{\mathbb{R}^d} d\mathbf{v}_* \frac{\Sigma - B_\Sigma}{\Sigma} \sum_{j=1}^{N} \mu_j^2 \, \delta\left(\mathbf{v} - \xi_j^n\right) \, \delta\left(\mathbf{v}_* - \xi_j^n\right) \\ &= \sum_{j=1}^{N} \int_{V_{\mathbf{k}}} d\mathbf{v} \, \mu_j^2 \, \frac{\Sigma - B_\Sigma\left(\left|\mathbf{v} - \xi_j^n\right|, \mathbf{n}\right)}{\Sigma} \, \delta\left(\mathbf{v} - \xi_j^n\right) \\ &= \sum_{j=1}^{N} \mu_j^2 \, \mathbb{1}_{\xi_j^n \in V_{\mathbf{k}}} \end{aligned}$$

where we used the trivial property: $B_\Sigma(0, \mathbf{n}) = 0$ (i.e. two particles with the same velocity cannot collide).

The term A_2 is given by:

$$\begin{aligned} A_2 &= \int_{V_{\mathbf{k}}} d\mathbf{v} \int_{\mathbb{R}^d} d\mathbf{v}_* \frac{\Sigma - B_\Sigma}{\Sigma} \sum_{k=1}^{N(N-1)/2} \hat{\mu}_k \, \delta\left(\mathbf{v} - \xi_k^n\right) \, \delta\left(\mathbf{v}_* - {\xi_*}_k^n\right) \\ &= \sum_{k=1}^{N(N-1)/2} \hat{\mu}_k \int_{V_{\mathbf{k}}} d\mathbf{v} \frac{\Sigma - B_\Sigma\left(\left|\mathbf{v} - {\xi_*}_k^n\right|, \mathbf{n}\right)}{\Sigma} \, \delta\left(\mathbf{v} - \xi_k^n\right) \\ &= \sum_{k=1}^{N(N-1)/2} \hat{\mu}_k \, \frac{\Sigma - B_{\Sigma k}}{\Sigma} \, \mathbb{1}_{\xi_k^n \in V_{\mathbf{k}}} \end{aligned}$$

where $B_{\Sigma k} = B_\Sigma\left(\left|\xi_k^n - {\xi_*}_k^n\right|, \mathbf{n}\right)$. Lastly, the term A_3 is defined as A_2 with ${\xi_*}_j^n$ and ξ_j^n exchanged.

$$\begin{aligned} A_3 &= \int_{V_{\mathbf{k}}} d\mathbf{v} \int_{\mathbb{R}^d} d\mathbf{v}_* \frac{\Sigma - B_\Sigma}{\Sigma} \sum_{k=1}^{N(N-1)/2} \hat{\mu}_k \, \delta\left(\mathbf{v} - {\xi_*}_k^n\right) \, \delta\left(\mathbf{v}_* - \xi_k^n\right) \\ &= \sum_{k=1}^{N(N-1)/2} \hat{\mu}_k \, \frac{\Sigma - B_{\Sigma k}}{\Sigma} \, \mathbb{1}_{{\xi_*}_k^n \in V_{\mathbf{k}}} \end{aligned}$$

Pertaining to term B_1, we get:

$$B_1 = \int_{V_{\mathbf{k}}} d\mathbf{v} \int_{\mathbb{R}^d} d\mathbf{v}_* \frac{B_\Sigma}{\Sigma} \sum_{j=1}^{N} \mu_j^2 \delta\left(\mathbf{v}' - \xi_j^n\right) \, \delta\left(\mathbf{v}_*' - \xi_j^n\right)$$

Before proceeding with integration in $d\mathbf{v}\, d\mathbf{v}_*$, we use the following identity which comes from the properties of the Dirac delta function:

$$\begin{aligned} \delta\left(\mathbf{v}' - \xi_j^n\right) \, \delta\left(\mathbf{v}_*' - \xi_j^n\right) &= \delta\left(\begin{pmatrix} \mathbf{v}' \\ \mathbf{v}_*' \end{pmatrix} - \begin{pmatrix} \xi_j^n \\ {\xi_*}_j^n \end{pmatrix}\right) \\ &= \delta\left(J\left(\begin{pmatrix} \mathbf{v} \\ \mathbf{v}_* \end{pmatrix} - J^{-1}\begin{pmatrix} \xi_j^n \\ {\xi_*}_j^n \end{pmatrix}\right)\right) \\ &= \frac{1}{|J|}\delta\left(\begin{pmatrix} \mathbf{v} \\ \mathbf{v}_* \end{pmatrix} - \begin{pmatrix} {\xi'}_j^n \\ {\xi'_*}_j^n \end{pmatrix}\right) = \delta\left(\mathbf{v} - {\xi'}_j^n\right) \, \delta\left(\mathbf{v}_* - {\xi'_*}_j^n\right) \end{aligned} \tag{37}$$

where ${\xi'}_j^n$ and ${\xi'_*}_j^n$ are the post-collisional velocities of $\left(\xi_j^n, {\xi_*}_j^n\right)$ with impact direction to be specified.

Using eq. (37), the term B_1 gives:

$$B_1 = \int_{V_{\mathbf{k}}} d\mathbf{v} \int_{\mathbb{R}^d} d\mathbf{v}_* \frac{B_\Sigma}{\Sigma} \sum_{j=1}^{N} \mu_j^2 \delta\left(\mathbf{v} - \xi_j^n\right) \delta\left(\mathbf{v}_* - \xi_j^n\right)$$
$$= \sum_{j=1}^{N} \mu_j^2 \int_{V_{\mathbf{k}}} d\mathbf{v} \frac{B_\Sigma\left(\left|\mathbf{v} - \xi_j^n\right|, \mathbf{n}\right)}{\Sigma} \delta\left(\mathbf{v} - \xi_j^n\right) = 0$$

where in the second equality we used again the identity $B_\Sigma(0, \mathbf{n}) = 0$.

Applying the same steps yielding (37) to B_2, one gets:

$$B_2 = \int_{V_{\mathbf{k}}} d\mathbf{v} \int_{\mathbb{R}^d} d\mathbf{v}_* \frac{B_\Sigma}{\Sigma} \sum_{k=1}^{N(N-1)/2} \hat{\mu}_k \delta\left(\mathbf{v} - {\xi'}_k^n\right) \delta\left(\mathbf{v}_* - {\xi'}_{*k}^n\right)$$
$$= \sum_{k=1}^{N(N-1)/2} \hat{\mu}_k \int_{V_{\mathbf{k}}} d\mathbf{v} \frac{B_\Sigma\left(\left|\mathbf{v} - {\xi'}_{*k}^n\right|, \mathbf{n}\right)}{\Sigma} \delta\left(\mathbf{v} - {\xi'}_k^n\right)$$
$$= \sum_{k=1}^{N(N-1)/2} \hat{\mu}_k \frac{B_\Sigma\left(\left|\xi_k^n - \xi_{*k}^n\right|, \mathbf{n}\right)}{\Sigma} \mathbb{1}_{{\xi'}_k^n \in V_{\mathbf{k}}}$$

where we used the property (4) of elastic collisions.

Lastly, the term B_3 has the same structure as B_2 with ξ_k^n and ξ_{*k}^n exchanged.

$$B_3 = \int_{V_{\mathbf{k}}} d\mathbf{v} \int_{\mathbb{R}^d} d\mathbf{v}_* \frac{B_\Sigma}{\Sigma} \sum_{k=1}^{N(N-1)/2} \hat{\mu}_k \delta\left(\mathbf{v}' - \xi_{*k}^n\right) \delta\left(\mathbf{v}'_* - \xi_k^n\right)$$
$$= \sum_{k=1}^{N(N-1)/2} \hat{\mu}_k \frac{B_\Sigma\left(\left|\xi_k^n - \xi_{*k}^n\right|, \mathbf{n}\right)}{\Sigma} \mathbb{1}_{{\xi'}_{*k}^n \in V_{\mathbf{k}}}$$

Replacing the values of A_i and B_i, $i = 1, 2, 3$ in eq (36) we get:

$$\begin{aligned}\int_{V_{\mathbf{k}}} \mathcal{P}\left({f_c}^n, {f_c}^n\right) d\mathbf{v} = &\sum_{j=1}^{N} \mu_j^2 \mathbb{1}_{\xi_j \in V_{\mathbf{k}}} \\ &+ \sum_{k=1}^{N(N-1)/2} \hat{\mu}_k \int_{\mathcal{S}^{d-1}} \frac{d\mathbf{n}}{4\pi} \left[\frac{\Sigma - B_{\Sigma k}(\mathbf{n})}{\Sigma} \mathbb{1}_{\xi_j^n \in V_{\mathbf{k}}} + \frac{\Sigma - B_{\Sigma k}(\mathbf{n})}{\Sigma} \mathbb{1}_{{\xi_*}_j^n \in V_{\mathbf{k}}}\right. \\ &\left. + \frac{B_{\Sigma k}(\mathbf{n})}{\Sigma} \mathbb{1}_{{\xi'}_j^n \in V_{\mathbf{k}}} + \frac{B_{\Sigma k}(\mathbf{n})}{\Sigma} \mathbb{1}_{{\xi'}_{*j}^n \in V_{\mathbf{k}}}\right]\end{aligned} \tag{38}$$

Integration in $d\mathbf{n}$ is performed using a Monte Carlo quadrature rule that is:

$$\int_\Omega \phi(x) \frac{d\Omega}{|\Omega|} \approx \frac{1}{M} \sum_{i=1}^{M} \phi(\chi_i) \tag{39}$$

where $\{\chi_i\}_{i=1,\ldots,M}$ is a set of M values sampled from a uniform distribution over the integration domain Ω.

If N_θ is the number of impact directions sampled for each candidate pair from a uniform distribution over the unit sphere, the relaxation step of the hybrid method becomes:

$$\int_{V_{\mathbf{k}}} \mathcal{P}\left(f_c{}^n,\, f_c{}^n\right) d\mathbf{v} = \sum_{j=1}^{N} \mu_j^2 \mathbb{1}_{\xi_j \in V_{\mathbf{k}}} + \sum_{k=1}^{N(N-1)/2} \hat{\mu}_k \frac{1}{N_\theta} \sum_{m=1}^{N_\theta} \left[\frac{B_{\Sigma k,m}}{\Sigma} \mathbb{1}_{\xi'^n_{j,m} \in V_{\mathbf{k}}} + \frac{B_{\Sigma k,m}}{\Sigma} \mathbb{1}_{\xi'^n_{*j,m} \in V_{\mathbf{k}}} + \frac{\Sigma - B_{\Sigma k,m}}{\Sigma} \mathbb{1}_{\xi_j^n \in V_{\mathbf{k}}} + \frac{\Sigma - B_{\Sigma k,m}}{\Sigma} \mathbb{1}_{\xi_{*j}^n \in V_{\mathbf{k}}} \right] \tag{40}$$

where $B_{\Sigma k,m} = B_\Sigma\left(\left|\xi_k^n - \xi_{*k}^n\right|, \mathbf{n}_{k,m}\right)$, and $\mathbf{n}_{k,m}$ is the m-th impact direction for the k-th couple. In the above equation $\xi'^n_{k,m}$ and $\xi'_{*k,m}$ are the post-collisional velocities of particles in the k-th couple with impact direction given by $\mathbf{n}_{k,m}$.

In the particular case $N_\theta = 1$ (a single impact direction chosen at random for each candidate pair), the final expression of the hybrid relaxation step (30) becomes:

$$f_{\mathbf{k}}^{n+1} = f_{\mathbf{k}}^n - \sum_{j=1}^{N} \frac{1}{\Delta v_{\mathbf{k}}} \left(\mu_j - \frac{\mu_j^2}{\rho_c^n}\right) \mathbb{1}_{\xi_j^n \in V_{\mathbf{k}}} + \sum_{k=1}^{N(N-1)/2} \frac{\hat{\mu}_k}{\rho_c^n \Delta v_{\mathbf{k}}} \left[\frac{B_{\Sigma k}}{\Sigma} \mathbb{1}_{\xi'^n_k \in V_{\mathbf{k}}} + \frac{B_{\Sigma k}}{\Sigma} \mathbb{1}_{\xi'^n_{*k} \in V_{\mathbf{k}}} + \frac{\Sigma - B_{\Sigma k}}{\Sigma} \mathbb{1}_{\xi_k^n \in V_{\mathbf{k}}} + \frac{\Sigma - B_{\Sigma k}}{\Sigma} \mathbb{1}_{\xi_{*k}^n \in V_{\mathbf{k}}} \right] \tag{41}$$

Eq. (41) can be interpreted as follows.

At the beginning of the relaxation step, a piecewise constant reconstruction of the solution, $f_{\mathbf{k}}^n$ is available, which can also be interpreted as a velocity histogram of particle velocity. Then, a set of N particles candidate for collisions is generated with a total mass equal to ρ_c^n. Particles velocity is sampled from the velocity histogram $f_{\mathbf{k}}^n$, but since each particle collides only once per time step, the sampling is performed without replacement. This is accomplished in the following manner: every time the velocity of a particle is sampled from the velocity cell $V_{\mathbf{k}}$, the value of $f_{\mathbf{k}}^n$ is deprived by the quantity $\frac{1}{\Delta \mathbf{v}_{\mathbf{k}}}\left(\mu_j - \frac{\mu_j^2}{\rho_c^n}\right)$.

Given the N particles candidate for collisions, all the $N\left(N-1\right)/2$ possible pairs are built. For each couple we sample the impact direction from a uniform distribution over the unit sphere, and the impact parameter B_Σ is evaluated for that couple of particles. Then collisions are performed and the value $f_{\mathbf{k}}^n$ is updated adding a contribution:

- $\frac{\hat{\mu}_k}{\rho_c^n \Delta v_{\mathbf{k}}} B_{\Sigma k}/\Sigma$ for each couple whose test particle has velocity $\xi'^n_k \in V_{\mathbf{k}}$ after the collision;
- $\frac{\hat{\mu}_k}{\rho_c^n \Delta v_{\mathbf{k}}} B_{\Sigma k}/\Sigma$ for each couple whose field particle has velocity $\xi'^n_{*k} \in V_{\mathbf{k}}$ after the collision;
- $\frac{\hat{\mu}_k}{\rho_c^n \Delta v_{\mathbf{k}}} \left(\Sigma - B_{\Sigma k}\right)/\Sigma$ for each couple whose test particle has velocity $\xi_k^n \in V_{\mathbf{k}}$ before the collision;
- $\frac{\hat{\mu}_k}{\rho_c^n \Delta v_{\mathbf{k}}} \left(\Sigma - B_{\Sigma k}\right)/\Sigma$ for each couple whose field particle has velocity $\xi_{*k}^n \in V_{\mathbf{k}}$ before the collision;

Roughly speaking, each candidate pair is considered at the same time as it were a colliding pair and not.

Note that (41) can also be interpreted as a projection of post-collisional velocities onto the velocity grid. Indeed, if a post-collisional velocity $\xi'^n_k \in V_{\mathbf{k}}$, thus the velocity histogram $f_{i,\mathbf{k}}$ is updated

by a certain quantity which is proportional to the collision probability so that the contribution of such a post-collisional velocity is 'condensed' into the grid nodes $\mathbf{v_k}$ (see also [30]).

Despite the hybrid algorithm looks similar to the DSMC method in §3, we have 3 major differences:

1. In the standard DSMC method, the solution of the relaxation step is represented by a set of particles whose velocities are updated during the relaxation step. On the contrary in the hybrid method the solution of the relaxation step is represented by a piecewise constant reconstruction of the solution which is then used as the initial data to deterministically solve the transport step.

2. In the standard DSMC method, the transport step is performed updating particle positions as described in §3.3. In the hybrid method the transport step is solved by a deterministic method.

3. In the standard DSMC method we have three kinds of particles. Particles which are not candidate for collisions, particles which are candidate for collisions but do not really collide, and candidate particles which actually collide. In the hybrid method the only particles present are candidate for collisions and they produce at the same time a contribution as colliding particles and a contribution as non-colliding particles.

4.2 Hybrid Method - Transport Step

At the end of the relaxation step a piecewise constant reconstruction of the velocity histogram is computed as suggested in eq. (41). This is used as initial data to deterministically solve the transport step.

In order to construct a deterministic numerical scheme for the transport step, we firstly introduce the bounded velocity space: $\mathbb{V} = \otimes_{m=1}^{d} \left[-V^{(m)}, V^{(m)}\right]$, where the lower/upper bounds on the m-th direction in the velocity space are chosen in such a way that $f_{i,\mathbf{k}}$ is negligibly small $\forall i, \mathbf{k}$ (Alternatively one can introduce upper/lower bounds which variy for each space cell).

Since the hybrid algorithm is only first order accurate, we use a first order upwind formula to compute numerical fluxes, so the numerical scheme for the transport step in a one dimensional problem reads as follows:

$$f_{i,\mathbf{k}}^{n+1} = f_{i,\mathbf{k}}^{n} - \frac{\Delta t}{\Delta x}\left(\mathcal{F}_{i+\frac{1}{2},\mathbf{k}}^{n} - \mathcal{F}_{i-\frac{1}{2},\mathbf{k}}^{n}\right), \quad i = 1, \ldots, N_x, \quad \mathbf{k} : \mathbf{v_k} \in \mathbb{V}, \tag{42}$$

Here $\mathcal{F}_{i+\frac{1}{2},\mathbf{k}}^{n}$ is the numerical flux evaluated in $x_{i+\frac{1}{2}}$, which is given by the upwind formula:

$$\mathcal{F}_{i+\frac{1}{2},\mathbf{k}}^{n} = \frac{v_{\mathbf{k}}^{(1)}}{2}\left(f_{i+1,\mathbf{k}}^{n} + f_{i,\mathbf{k}}^{n}\right) - \frac{\left|v_{\mathbf{k}}^{(1)}\right|}{2}\left(f_{i+1,\mathbf{k}}^{n} - f_{i,\mathbf{k}}^{n}\right) \tag{43}$$

and $v_{\mathbf{k}}^{(1)}$ is the first component of velocity $\mathbf{v_k}$ associated with the $\mathbf{k}$-th grid node.

In order to have L^1-stability, the following restriction on the time step must be imposed (CFL condition):

$$\Delta t \leq \frac{\min_{1=1,\ldots,N_x} \Delta x_i}{V^{(1)}} \tag{44}$$

4.3 Hybrid Method - Positivity of the solution

Algorithm 4.1 *Sampling without replacement*

- *Given the velocity histogram* $f_{\boldsymbol{k}}^n$ *compute the cumulative density distribution:* $F_{\boldsymbol{k}} := \sum_{\mathbf{i}\leq \boldsymbol{k}} \frac{1}{\rho^n} f_{\mathbf{i}}^n \Delta v_{\mathbf{i}}$
- *for* $j = 1, \dots, N$
  - *extract at random a number* $\varepsilon \in [0,1]$
  - *find* $\mathbf{j} : F_{\mathbf{j}-1} < \varepsilon \leq F_{\mathbf{j}}$
  - *set* $\xi_j^n \leftarrow \boldsymbol{v}_{\mathbf{j}}$ *and* $m = \mu - \frac{\mu^2}{\rho_c^n}$
  - *Update the density value:* $\rho^n \leftarrow \rho^n - \mu$
  - *Update the density distribution:* $f_{\mathbf{j}}^n \leftarrow f_{\mathbf{j}}^n - \frac{m}{\Delta v_{\mathbf{j}}}$
  - *Update the cumulative density distribution:*

$$F_{\boldsymbol{k}} \leftarrow \begin{cases} \dfrac{\rho^n + m}{\rho^n} F_{\boldsymbol{k}} & \text{if } \boldsymbol{k} < \mathbf{j} \\ \dfrac{\rho^n + m}{\rho^n} F_{\boldsymbol{k}} - \dfrac{m}{\rho^n} & \text{if } \boldsymbol{k} \geq \mathbf{j} \end{cases}$$

- *end*

In this section we will discuss one of the key property of the hybrid scheme: the positivity of the solution. To this purpose we firstly rewrite the hybrid relaxation step in a contracted form:

$$f_{\mathbf{k}}^{n+1} = {f_{nc}}_{\mathbf{k}}^{n} + {f_c}_{\mathbf{k}}^{n+1} \tag{45}$$

where:

$${f_{nc}}_{\mathbf{k}}^{n} = \sum_{j=1}^{N} \frac{1}{\Delta v_{\mathbf{k}}} \left(\mu_j - \frac{\mu_j^2}{\rho_c^n} \right) \mathbb{1}_{\xi_j^n \in V_{\mathbf{k}}}$$

From eq. (45) we deduce that if both ${f_c}^{n+1}$ and ${f_{nc}}^{n}$ are non-negative thus also the solution at time t^{n+1} is non-negative.

Non-negativity of ${f_c}^{n+1}$ immediately follows from the definition of Σ as the upper bound for the impact parameter, and from the fact that the modified impact parameter B_Σ is a non-negative function. Thus we have that ${f_c}_{\mathbf{k}}^{n+1}$ is given by a convex combination of non-negative terms and therefore it is non-negative.

On the contrary, ${f_{nc}}_{\mathbf{k}}^{n}$ represents the velocity histogram of particles which are not candidate for collisions, that is the remaining part of $f_{\mathbf{k}}^n$ after the N candidate particles are generated at the beginning of the relaxation step. Thus the positivity of ${f_{nc}}_{\mathbf{k}}^{n}$ is strictly linked to the sampling algorithm used to generate the particle set.

Let us start presenting the basic algorithm for sampling N velocity values without replacement from f (algorithm 4.1). The sampling algorithm is outlined at the beginning of this section, and it is assumed that all particles have equal mass μ (as customary in the standard DSMC method).

From the algorithm 4.1, it is clear that if $f_{\mathbf{k}}^n = 0$, thus $F_{\mathbf{k}+1}^n = F_{\mathbf{k}}^n$ and the probability to sample a velocity value from the cell $V_{\mathbf{k}}$ is zero. However, it could happen that $0 < f_{\mathbf{k}}^n < \left(\mu - \frac{\mu^2}{\rho_c^n}\right)/\Delta v_{\mathbf{k}}$. In such cases the probability to assign the velocity value $\mathbf{v_k}$ to the j-th particle is non zero and

consequently the difference $f_{\mathbf{k}}^n - \left(\mu - \frac{\mu^2}{\rho_c^n}\right)/\Delta v_{\mathbf{k}} < 0$, i.e. ${f_{nc}}_{\mathbf{k}}^n < 0$ and positivity of the solution is not ensured.

In order to overcome this difficultly, one can modify the sampling algorithm as follows: the velocity value $\mathbf{v_k}$ is sampled only if $f_{\mathbf{k}}^n > \left(\mu - \frac{\mu^2}{\rho_c^n}\right)/\Delta v_{\mathbf{k}}$, so that the positivity of ${f_{nc}}_{\mathbf{k}}^n$ is ensured. However there are two main drawbacks inherent in such an approach.

The first inconvenient relies in the fact that if the numerical value of μ is too large, no velocity values are sampled from the tails of the distribution and the relaxation process would be inhibited.

Pertaining to the second inconvenient, we have that for a fixed value of μ, one can estimate *a priori* both the number of particles candidate for collisions, and the maximum number of velocity values that can be sampled from the velocity histogram $f_{\mathbf{k}}^n$ without losing the non-negativity of ${f_{nc}}_{\mathbf{k}}^n$. The number of particles candidate for collisions at time t^n is $N = 2{N_c}^n$ where ${N_c}^n$ is given by (21). The maximum number of velocity values that can be sampled without replacement from $f_{\mathbf{k}}^n$ without losing the non-negativity of ${f_{nc}}_{\mathbf{k}}^n$ is given by:

$$N_{\max} = \sum_{\mathbf{k}} \left\lfloor \frac{1}{\mu} f_{\mathbf{k}}^n \Delta v_{\mathbf{k}} \right\rfloor$$

where $\lfloor x \rfloor$ is the rounding down of the real x.

The problem is that there is no reason why it should be $N < N_{\max}$, i.e. it could happen that the number of candidate particles required to correctly solve the relaxation step is greater than the number of velocity values that can be sampled without replacement from the velocity histogram $f_{\mathbf{k}}^n$.

Since the estimate (21) depends on Δt, one could artificially reduce the time step in order to have $N_{\max} > N$. However the break even point could occur for very low values (even zero) of Δt.

For the previous reasons, we opt for the possibility of assigning to each particle a different mass, i.e. when the velocity value for the **j**-th particle is sampled from the velocity cell $V_{\mathbf{k}}$, we set:

$$\mu_j = \min\left\{\max\left\{m_l,\, f_{\mathbf{k}}^n \Delta v_{\mathbf{k}}\right\}, m_u\right\} \tag{46}$$

where m_l is a lower bound to avoid too small values for the particle mass, while m_u is an upper bound to avoid large values for the particle mass.

In our numerical tests the lower bound for the particle mass was set to the machine precision value, while m_u actually worked as a discretization parameter, so that the number of particles sampled is linked to both the numerical value of m_u and the number of velocity cells.

The resulting algorithm is outlined at the end of the present section.

Using the sampling algorithm 4.2, the non-negativity of ${f_{nc}}_{\mathbf{k}}^n$ is preserved. Indeed:

- if $f_{\mathbf{k}}^n \Delta v_{\mathbf{k}} < m_l$, thus the mass of particles with velocity in V_k is negligibly small and no velocity values are sampled;
- if $m_l < f_{\mathbf{k}}^n \Delta v_{\mathbf{k}} < m_u$, thus $\mu_j = f_{\mathbf{k}}^n / \Delta v_{\mathbf{k}}$ and ${f_{nc}}_{\mathbf{k}}^n = f_{\mathbf{k}}^n - \left(\mu_j - \frac{\mu_j^2}{\rho_c^n}\right)/\Delta v_{\mathbf{k}} > 0$
- lastly, if $f_{\mathbf{k}}^n \Delta v_{\mathbf{k}} > m_u$, thus $\mu_j = m_u$ and again ${f_{nc}}_{\mathbf{k}}^n > 0$

Algorithm 4.2 *Sampling without replacement - modified algorithm*

- *Given the velocity histogram* $f^n_{\boldsymbol{k}}$ *compute the cumulative density distribution:* $F_{\boldsymbol{k}} := \sum_{\mathbf{i}\le \boldsymbol{k}} \frac{1}{\rho^n} f^n_{\mathbf{i}} \Delta v_{\mathbf{i}}$
- *Set:* $mass = 0$ *and* $j = 0$
- *while* $mass < \rho^n_c$
  - *extract at random a number* $\varepsilon \in [0,1]$
  - *find* $\mathbf{j} : F_{\mathbf{j}-1} < \varepsilon \le F_{\mathbf{j}}$
  - *if* $f^n_{\mathbf{j}} > \frac{m_l}{\Delta v_{\mathbf{j}}}$
    - *update:* $j \leftarrow j+1$
    - *set:* $\mu_j = \min\{m_u,\, f_{\mathbf{j}} \Delta v_{\mathbf{j}}\}$ *and* $m = \mu_j - \frac{\mu_j^2}{\rho^n_c}$
    - *set* $\xi^n_j \leftarrow \boldsymbol{v}_{\mathbf{j}}$
    - *update:* $mass \leftarrow mass + \mu_j$
    - *update density:* $\rho^n \leftarrow \rho^n - \mu_j$
    - *Update the density distribution:* $f^n_{\mathbf{j}} \leftarrow f^n_{\mathbf{j}} - \frac{m}{\Delta v_{\mathbf{j}}}$
    - *Update the cumulative density distribution:*

$$F_{\boldsymbol{k}} \leftarrow \begin{cases} \dfrac{\rho^n + m}{\rho^n} F_{\boldsymbol{k}} & \text{if } \boldsymbol{k} < \mathbf{j} \\ \dfrac{\rho^n + m}{\rho^n} F_{\boldsymbol{k}} - \dfrac{m}{\rho^n} & \text{if } \boldsymbol{k} \ge \mathbf{j} \end{cases}$$

  - *end*
- *end*

4.4 Hybrid method - Projection step

It is easy to prove that the hybrid method (41) is exactly conservative with respect to mass. If further the velocity grid is uniform, the hybrid method is exactly conservative also with respect to momentum. However we have a lack in energy conservation, which means that at each relaxation step we have a spurious contribution on the total energy which is due to approximating post-collisional velocities with grid nodes.

In order to overcome this difficulty, we propose to project post-collisional velocities onto the velocity grid in a conservative way, i.e. we split the contribution of each post-collisional velocity onto a set of grid nodes in such a way that mass, momentum and energy are preserved. A similar approach can be found in [30] where post-collisional velocities are also projected onto a fixed velocity grid when the collisional integral is evaluated. We think however that the present approach is simpler.

The projection method we are going to present, can be applied in case of a uniform discretization of the velocity space. Let $N_v^{(\alpha)}$ be the number of grid nodes along the α-th direction of the velocity space, $\alpha = 1, \dots, d$, and $\Delta v^{(\alpha)}$ be the grid spacing along that direction. We denote with the symbol $v^{(\alpha)}_{k^{(\alpha)}}$ the $k^{(\alpha)}$-th grid node, $k^{(\alpha)} = 1, \dots, N_v^{(\alpha)}$. Lastly, we denote with the symbol $\mathbf{k}$ the multi-index $\mathbf{k} = \left(k^{(1)}, \dots, k^{(d)}\right)$ so that $\mathbf{v_k} = \left(v^{(1)}_{k^{(1)}}, \dots, v^{(d)}_{k^{(d)}}\right)$.

Given the post-collisional velocity of the test particle in the k-th couple, we choose a subset of

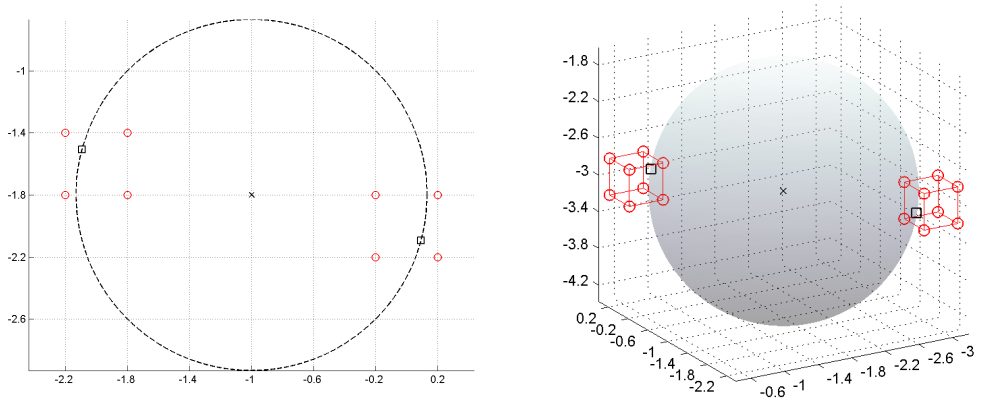

Figure 2: Projection stencil (circles) for a pair of post-collisional velocities (squares) in the case of two (left) and three (right) dimensions in the velocity space

grid nodes on which the contribution of the post-collisional velocity will be splitted. We will refer to such set of nodes as *projection stencil*. The projection stencil for ξ'^n_k will be indicated as $\mathcal{K}_k$ and it is composed of 2^d nodes chosen with the following criterion. For each direction in the velocity space we set $j^{(\alpha)} \in \left\{1, \ldots, N_v^{(\alpha)}\right\} : \left(\xi'^n_k\right)^{(\alpha)} \in \left[\left(j^{(\alpha)} - \frac{1}{2}\right)\Delta v^{(\alpha)}, \left(j^{(\alpha)} + \frac{1}{2}\right)\Delta v^{(\alpha)}\right]$. Then we define:

$$\mathcal{K}_k^{(\alpha)} = \begin{cases} \left\{j^{(\alpha)}, j^{(\alpha)} + 1\right\} & \text{if } \left(\xi'^n_k\right)^{(\alpha)} > v_j^{(\alpha)} \\ \left\{j^{(\alpha)}, j^{(\alpha)} - 1\right\} & \text{if } \left(\xi'^n_k\right)^{(\alpha)} < v_j^{(\alpha)} \end{cases} \tag{47}$$

The projection stencil for ξ'^n_k is finally given by $\mathcal{K}_k = \otimes_{\alpha=1}^d \mathcal{K}_k^{(\alpha)}$ and the set of grid nodes on which ξ'^n_k will be projected is $\mathcal{V}_k = \{\mathbf{v_j} : \mathbf{j} \in \mathcal{K}_k\}$.

Since the conservation of momentum is automatically achieved by projecting in a symmetrical way the post-collisional velocities in the same pair, we define the projection stencil for the field particle as follows: $\mathcal{V}_{*k} = \{\mathbf{v_{j_*}} : \mathbf{v_{j_*}} = 2\mathbf{v}_m - \mathbf{v_j} \quad \forall \mathbf{j} \in \mathcal{K}_k\}$, where $\mathbf{v}_m = \frac{1}{2}\left(\xi'^n_k + \xi'^n_{*k}\right)$.

Two examples of projection stencils are shown in fig.2 for the case $d = 2$ (left) and $d = 3$ (right).

We associate each grid node in the projection stencil $\mathcal{V}_k$ with a weight $\Psi_{k,\mathbf{j}}$, and also the projection weights are symmetrically allocated on the projection stencil of the field particle $\mathcal{V}_{*k}$. For instance if we consider the k-th couple of candidate particles, the weight associated with the first node in $\mathcal{V}_k$ is also associated with the first node in $\mathcal{V}_{*k}$.

Since both the projection stencil and the weights are symmetric, conservation of momentum is automatically achieved, thus the projection weights are determined by imposing conservation of mass and energy only:

$$\begin{cases} \sum_{\mathbf{j} \in \mathcal{K}_k} \Psi_{k,\mathbf{j}} = 1 \\ \sum_{\mathbf{j} \in \mathcal{K}_k} \Psi_{k,\mathbf{j}} \left|\mathbf{v_j} - \mathbf{v}_m\right|^2 = \left|\xi'^n_k - \mathbf{v}_m\right|^2 \end{cases} \tag{48}$$

The system (48) is a two equations system with 2^d unknowns to be solved in a least square sense. We start proving that (48) is indeed a consequence of mass and energy conservation.

Proposition 4.3 *The system* (48) *is equivalent to:*

$$\begin{cases} \displaystyle\sum_{\mathbf{j}\in\mathcal{K}_k} \Psi_{k,\mathbf{j}} = 1 \\ \displaystyle\sum_{\mathbf{j}\in\mathcal{K}_k} \Psi_{k,\mathbf{j}} {\boldsymbol{v}_{\mathbf{j}}}^2 + \sum_{\mathbf{j}_*\in\mathcal{K}_{*k}} \Psi_{k,\mathbf{j}_*} {\boldsymbol{v}_{\mathbf{j}_*}}^2 = \left|{\xi'}_j^n\right|^2 + \left|{\xi'}_{*j}^n\right|^2 \end{cases}$$

Proof.

Since we impose that $\mathcal{V}_{*k}$ is the symmetrical of $\mathcal{V}_k$ with respect to $\mathbf{v}_m$, we have that $\mathbf{v}_{\mathbf{j}_*} = 2\mathbf{v}_m - \mathbf{v}_{\mathbf{j}}$, $\forall \mathbf{j}_* \in \mathcal{K}_{*k}$; Moreover since also the projection weights are symmetrically allocated on the projection stencils, the second equation in (48) becomes:

$$\sum_{\mathbf{j}_*\in\mathcal{K}_{*k}} \Psi_{k,\mathbf{j}_*} \left|\mathbf{v}_m - \mathbf{v}_{\mathbf{j}_*}\right|^2 = \left|\mathbf{v}_m - {\xi'}_{*k}^n\right|^2$$

and we used also the point-symmetry of post-collisional velocities with respect to $\mathbf{v}_m$.

Adding the previous equation to the second equation in (48) we get:

$$\sum_{\mathbf{j}\in\mathcal{K}_k} \Psi_{k,\mathbf{j}} \left|\mathbf{v}_m - \mathbf{v}_{\mathbf{j}_*}\right|^2 + \sum_{\mathbf{j}_*\in\mathcal{K}_{*k}} \Psi_{k,\mathbf{j}_*} \left|\mathbf{v}_m - \mathbf{v}_{\mathbf{j}_*}\right|^2 = \left|\mathbf{v}_m - {\xi'}_{*k}^n\right|^2 + \left|\mathbf{v}_m - {\xi'}_{*k}^n\right|^2$$

from which we deduce the thesis with simple algebraic manipulations.

■

With a simple analysis, it is possible to show that the projection weights can be chosen in [0, 1], so that non-negativity of the solution is ensured.

With the projection method described in this section, the relaxation step of the hybrid method (41) becomes:

$$\begin{aligned} f_{\mathbf{k}}^{n+1} = f_{\mathbf{k}}^n &- \frac{1}{\Delta\mathbf{v}_{\mathbf{k}}} \sum_{j=1}^{N} \left(\mu_j - \frac{\mu_j^2}{\rho_c^n}\right) \mathbb{1}_{\xi_j^n \in V_{\mathbf{k}}} \\ &+ \sum_{k=1}^{N(N-1)/2} \frac{\hat{\mu}_k}{\Delta v_{\mathbf{k}} \rho_c^n} \left[\sum_{\mathbf{j}\in\mathcal{K}_k} \Psi_{k,\mathbf{j}} \frac{B_{\Sigma k}}{\Sigma} \mathbb{1}_{\mathbf{j}=\mathbf{k}} + \sum_{\mathbf{j}_*\in\mathcal{K}_{*k}} \Psi_{k,\mathbf{j}_*} \frac{B_{\Sigma k}}{\Sigma} \mathbb{1}_{\mathbf{j}_*=\mathbf{k}} \right. \\ &\left. + \frac{\Sigma - B_{\Sigma k}}{\Sigma} \mathbb{1}_{\xi_k^n \in V_{\mathbf{k}}} + \frac{\Sigma - B_{\Sigma k}}{\Sigma} \mathbb{1}_{{\xi_*}_k^n \in V_{\mathbf{k}}} \right] \end{aligned} \tag{49}$$

Proposition 4.4 *The hybrid method* (49) *is exactly conservative with respect to mass, momentum and energy, provided that a uniform discretization of the velocity space is used.*

Proof. The proof relies on simple calculations, and uses the properties of elastic collisions and proposition 4.3 ■

5 Numerical results

In this section we report some numerical results for both the space homogeneous and the one-dimensional problems. In both cases we consider a two dimensional velocity space ($d = 2$, corresponding to particles with two translational degrees of freedom). Numerical results for the hybrid scheme are compared with numerical results provided by the Nanbu-Babowski scheme described in §3.

	d	kn	Σ	m_u
NB	2	$10^{-2}, 1$	14.14	-
Hyb	2	$10^{-2}, 1$	14.14	10^{-2}

Table 1: Scheme parameters for space homogeneous test cases

5.1 Space homogeneous problem

In order to demonstrate that the hybrid method is able to reproduce a relaxation dynamic consistent with the Boltzmann equation, we consider the following space homogeneous problem.

Test 1. The initial data is given by the sum of two Maxwellian as in (26).
Test 2. The initial data is given by the sum of two half-Maxwellian:

$$\rho_1 = 0.5,\, \mathbf{u}_1 = (-1,\, 0)^T,\, T_1 = 1; \quad \rho_2 = 0.25,\, \mathbf{u}_2 = (2,\, 0)^T,\, T_2 = 1;$$
$$f\left(x, \mathbf{v}, t=0\right) = \begin{cases} \mathcal{M}_f\left[\rho_1, \mathbf{u}_1, T_1\right], & \mathbf{v}^{(1)} \leq \mathbf{u}^{(1)} \\ 0, & \text{otherwise} \end{cases} + \begin{cases} \mathcal{M}_f\left[\rho_2, \mathbf{u}_2, T2\right] & \mathbf{v}^{(1)} > \mathbf{u}^{(1)} \\ 0, & \text{otherwise} \end{cases} \tag{50}$$

and the exact solution for time approaching to infinity is the Maxwellian defined by: $\rho = 3/8$, $U = \left(-\frac{2}{3}\frac{1}{\sqrt{2\pi}},\, 0\right)$ and $T = 2 + \frac{8}{3\sqrt{2\pi}} - \frac{1}{9\pi}$.

In both previous tests we chose the final integration time $t_{max} = 10\, Kn$, so that at the final time the solution has already relaxed toward the reference equilibrium.

Numerical results provided by the hybrid method are compared with those provided by the NB scheme. For both test cases the scheme parameters are reported in table 1 (dimensionless variables).

The integration time step Δt is chosen in order to have $p = 0.1$ with the numerical values of parameters reported in table 1. This particular choice is motivated by the fact we are interested in solving the Boltzmann equation in kinetic regimes, which are characterized by large values of the Knudsen number. In such cases the time step restriction due to the transport step is much more restrictive then the time step restriction due to the relaxation step resulting in small values for p.

In the hybrid method we consider a uniform discretization of the bounded velocity space $\mathbb{V} = [-10, 10] \times [-10, 10]$ with 50 cells on each direction. The same discretization of the velocity space is used to evaluate the velocity histograms obtained with the NB scheme at final time.

Finally, the number of particles simulated by the Nanbu-Babowski scheme is set to the values $N = 10^3, 10^4$ (configurations NB1 and NB2 respectively).

In fig. 3 and 5, we report the L^1 norm of the difference between the solution provided by each method and the reference equilibrium for test 1 and test 2 respectively. As shown in both figures, the time behavior of such an error is characterized by two phases. The first phase represents the relaxation toward the reference equilibrium. The second part shows the error at the end of the relaxation process. Note that at steady state, the error between the solution and the reference equilibrium is not zero mainly because of stochastic fluctuations. The magnitude of such fluctuations reduces as the number of particles increases, so also the error at steady state reduces for large values of N.

As shown in fig. 3 and 5 the hybrid method is able to reproduce the same relaxation dynamic of the NB scheme, for both test cases. Moreover the error between the solution and the reference equilibrium produced by the hybrid method with roughly 25 candidate particles is comparable if not lower, with the error produced by the NB2 scheme with a greater number of particles.

This is confirmed in fig. 4 and 6, where velocity histograms provided by both methods are compared with the reference equilibrium for both test cases. Note that the stochastic noise on the velocity histogram provided by the hybrid method is of the same order as the stochastic noise

produced by NB2 scheme. On the contrary the results obtained with the NB1 scheme are affected by relevant stochastic noise.

Finally in tables from 2 to 5 we report the CPU time for both test cases for both Knudsen numbers. More specifically we report the average CPU time per time step associated with the sampling, collision and projection steps (2nd, 3rd and 4th columns), we report also the average number of candidate particles used during the relaxation step (1st column) and the overall CPU time required to complete the whole simulation (last column).

In both test cases, most of the CPU time spent by the hybrid method is due to the projection step, and the error on the steady solution in the hybrid scheme is comparable with the error of the NB2 scheme. However the CPU time are slightly greater, so the convenience of the hybrid algorithm in the space homogeneous problem is not particularly evident.

However in the 1D test case results will be significantly different. In fact in DSMC algorithm after the transport step, particles must be re-organized in a list which gives the index of particles within each space cell. This step task can be accomplished with at a cost of abut $N \log N$ operations (where N is the number of particles in the DSMC simulation). Conversely in the hybrid scheme the transport step is deterministically solved, so the CPU time required to solve the transport step in the hybrid algorithm is much smaller. More important, since no particles are advected in the hybrid scheme, no amplification of the stochastic noise on macroscopic profile is detected, resulting in a smother solution.

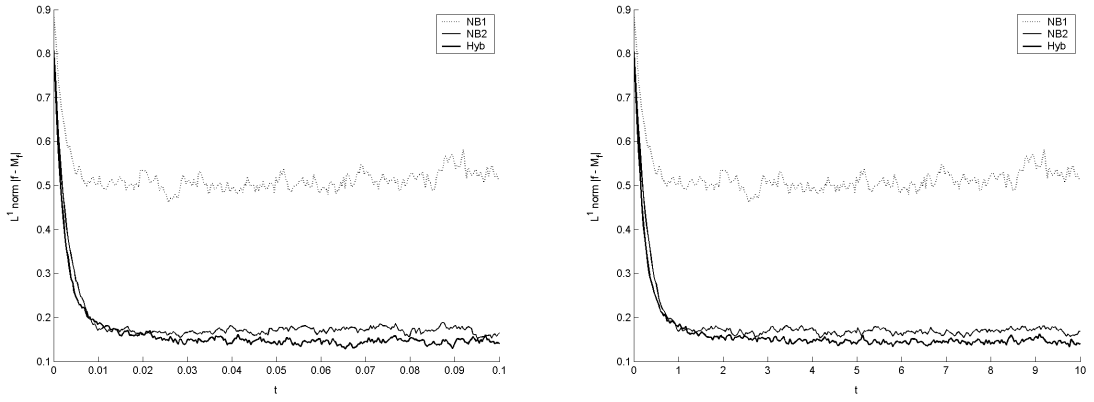

(a) $kn = 10^{-2}$ (b) $kn = 1$

Figure 3: **Test case 1**. Relaxation error

	N	sampl.	coll.	proj.	overall
NB1	100	0.0009	0.0002	-	13.4
NB2	1000	0.0106	0.0009	-	58.4
Hyb	24.4	0.0141	0.0003	0.0031	87.4

Table 2: CPU time [sec.] for test 1, $kn = 10^{-2}$

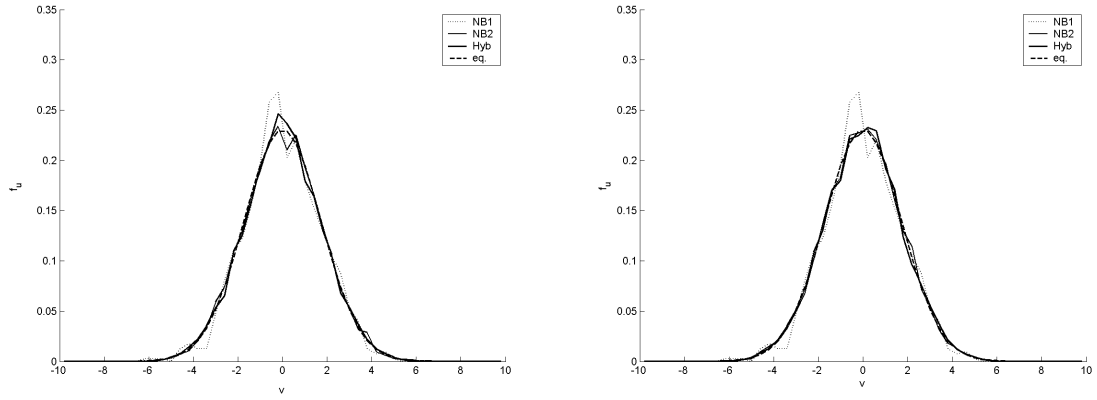

(a) $kn = 10^{-2}$ (b) $kn = 1$

Figure 4: **Test case 1**. Velocity histogram of the first component of the microscopic velocity at final time

	N	sampl.	coll.	proj.	overall
NB1	100	0.0008	0.0001	-	17.1
NB2	1000	0.0101	0.0009	-	59.5
Hyb	24.2	0.0130	0.0006	0.0030	85.4

Table 3: CPU time [sec.] for test 1, $kn = 1$

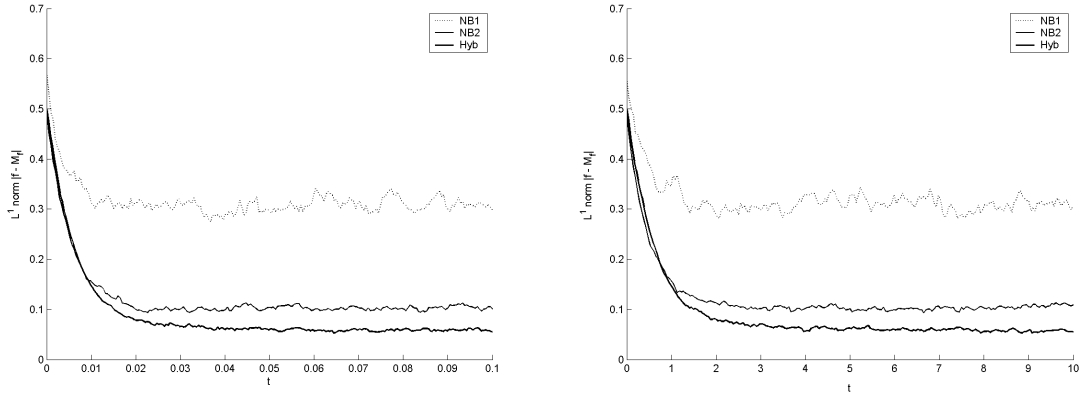

(a) $kn = 10^{-2}$ (b) $kn = 1$

Figure 5: **Test case 2**. Relaxation error

	N	sampl	coll	proj	overall
NB1	100	0.0005	0.0005	-	9.9
NB2	1000	0.0092	0.0007	-	43.9
Hyb	21.8	0.0156	0.0005	0.0026	75.2

Table 4: CPU times [sec.] for test 2, $kn = 10^{-2}$

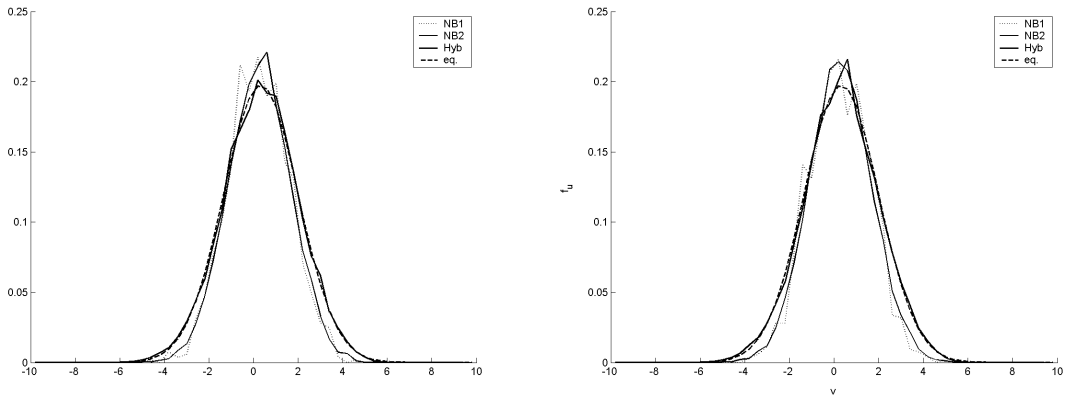

(a) $kn = 10^{-2}$ (b) $kn = 1$

Figure 6: **Test case 2**. Velocity histogram of the first component of the microscopic velocity at final time

	N	sampl	coll	proj	overall
NB1	100	0.0006	0.0002	-	11.3
NB2	1000	0.0097	0.0012	-	45.1
Hyb	22.1	0.0117	0.0003	0.0027	74.1

Table 5: CPU times [sec.] for test 2, $kn = 1$

5.2 1D test cases

In this section we report some numerical results for one-dimensional problems and two dimensions in velocity space. In all tests the physical domain is given by the interval $\mathcal{D} = [0, 1]$, while the velocity domain is again $\mathbb{V} = [-10, 10] \times [-10, 10]$.

In all cases the initial data has the form:

$$\begin{aligned} f(x, \mathbf{v}, t = 0) &= \mathcal{M}_f[\rho, \mathbf{u}, T] \\ (\rho, \mathbf{u}, T) &= \begin{cases} (\rho_L, \mathbf{u}_L, T_L), & \text{if } x < 0.5 \\ (\rho_R, \mathbf{u}_R, T_R), & \text{if } x \geq 0.5 \end{cases} \end{aligned} \tag{51}$$

where $\rho_L, \mathbf{u}_L, T_L$ and $\rho_R, \mathbf{u}_R, T_R$ are chosen according to the specific problem.

Test 3. Firstly we consider the *shock tube problem* with the following initial data:

$$\begin{aligned} &\rho_R = 1.0, && \rho_L = 0.1; \\ &U_R = U_L = 0.0; && \\ &T_R = 1.0, && T_L = 0.125 \end{aligned} \tag{52}$$

For small values of the Knudsen number the solution is characterized by a shock, a contact discontinuity and a rarefaction wave. For large Knudsen numbers the 3-waves-structure is loosen and macroscopic profiles are smeared out as the results of the gas rarefaction .

Test 4. We consider the following initial data

$$\begin{aligned} &\rho_R = 1.0, \qquad \rho_L = 0.9; \\ &U_R = U_L = 0.0; \\ &T_R = T_L = 1.0 \end{aligned} \tag{53}$$

which corresponds again to a *shock tube problem* with a weak contact discontinuity. This problem represents an acoustic perturbation.

Test 5 Lastly we consider the initial data:

$$\begin{aligned} &\rho_R = \rho_L = 1.0; \\ &U_R = -2.0, \qquad U_L = 2.0; \\ &T_R = T_L = 1.0 \end{aligned} \tag{54}$$

whose solution is characterized by two rarefaction waves moving in opposite directions, symmetrically with respect to the axes $x = 0.5$. The rarefaction waves produce an extremely rarefied region in the middle of the computational domain.

In all cases we consider a uniform discretization of the physical space with 100 cells, while each direction of the velocity space is discretized in 50 cells with uniform width.

The same discretization of the physical space is used in the NB scheme, while the velocity grid is used only to evaluate the velocity histograms at the final time at $x = 0.5$

Lastly in both schemes the numerical value of Σ is set to the same value as in the space homogeneous cases.

The following results refer to the case $Kn = 1$. As pointed out in the beginning of the present paper, this choice is motivated by the fact that in the framework of a domain decomposition approach, we are interested in using the hybrid scheme to solve the Boltzmann equation in fully kinetic regimes only.

In the following figures we report the comparison between results provided by the hybrid scheme, and results provided by the NB scheme. The number of particles used by the NB scheme is set to $10^4, 10^6$ particles in the whole computational domain (configuration NB3 and NB4 respectively).

In figs. 7, 9 and 11, we report density and temperature profiles provided by both schemes for Test 3, 4 and 5 respectively. In figs. 8, 10, we report the velocity histograms computed for the first component of the microscopic velocity at the final time in $x = 0.5$ for test case 3 and 4.

Lastly in tables 6, 7 and 8 we compare the CPU times required by both schemes. More specifically in the first column we report the average number of candidate particles used by both schemes, in columns from 2 to 4 we report the average CPU time per time step for the relaxation and transport step and the overall CPU time required for each simulation.

Numerical results show that in all cases the solution computed with the hybrid scheme is in good agreement with the solution of the NB4 scheme, but the quality of the solution is considerably improved. The reduction of the stochastic noise is particularly evident in test 4, where the magnitude of stochastic fluctuations obtained by the NB3 scheme is greater then the magnitude of the perturbation on density and temperature one wishes to compute, and the NB4 solution is definitely worse than the solution obtained with the hybrid scheme.

Also in test 5, the hybrid scheme is able to correctly catch the rarefied region around $x = 0.5$, better than the NB3 scheme.

Lastly as shown in figs. 8 and 10 the reduction of stochastic noise is relevant also at the microscopic level. Here stochastic fluctuations obtained with the hybrid method are again in the same order of those obtained with the NB4 scheme.

Pertaining to the computational time, we observe that in test 3 the total CPU time used by the hybrid scheme is approximatively 25% of the CPU time required by the NB4 scheme and the solution is smoother. In the remaining cases the CPU time is approximatively 50% of the CPU time required by the NB4 scheme, but the quality of the solution is considerably improved

The different contributions to the CPU time confirm that the hybrid relaxation step is more expensive than in the NB scheme, on the contrary the transport step requires less CPU time if compared with the NB scheme as in the hybrid algorithm no particles are transported and thus one does not need to re-allocate particles in each space cell.

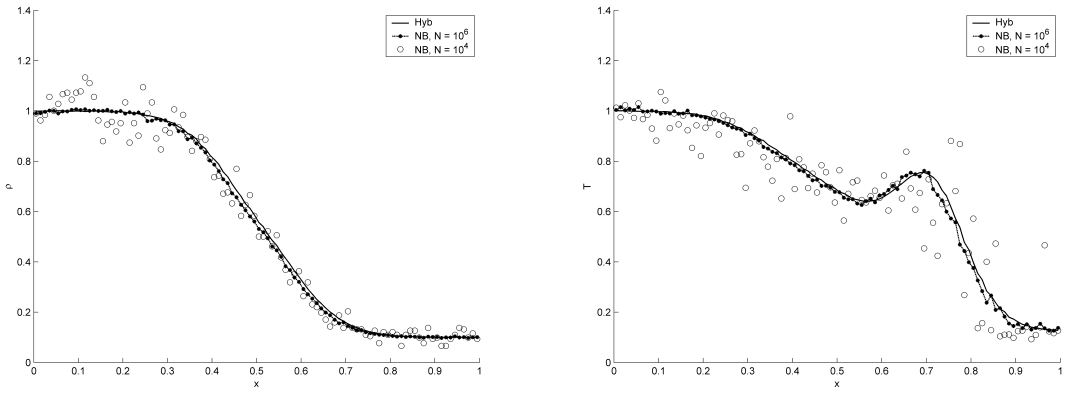

(a) Density profile

(b) Temperature profile

Figure 7: Test case 3, $Kn = 1$, $t = 0.12$. Density and temperature profiles for the NB3 scheme (circles), NB4 scheme (dotted line), and the hybrid algorithm (continuous line)

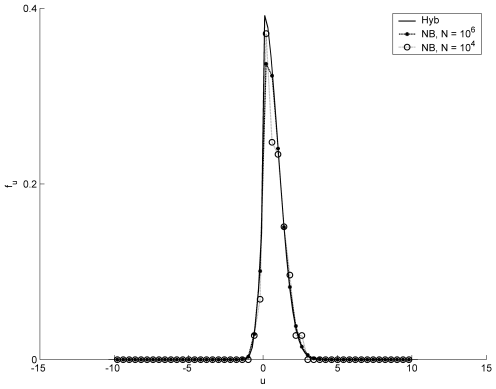

Figure 8: **Test case 3**. Velocity histogram with respect to the first component of the microscopic velocity in $x = 0.5$ at $t = 0.12$ for the NB3 scheme (circles), NB4 scheme (dotted line), and for the hybrid algorithm (continuous line)

	N	relax.	trans.	overall
NB3 (10^4 particles)	174	0.0160	0.0310	14.2
NB4 (10^6 particles)	22,314	0.2350	4.0780	637.2
Hyb	176	1.0160	0.1710	176.8

Table 6: CPU times [sec.] for test 3

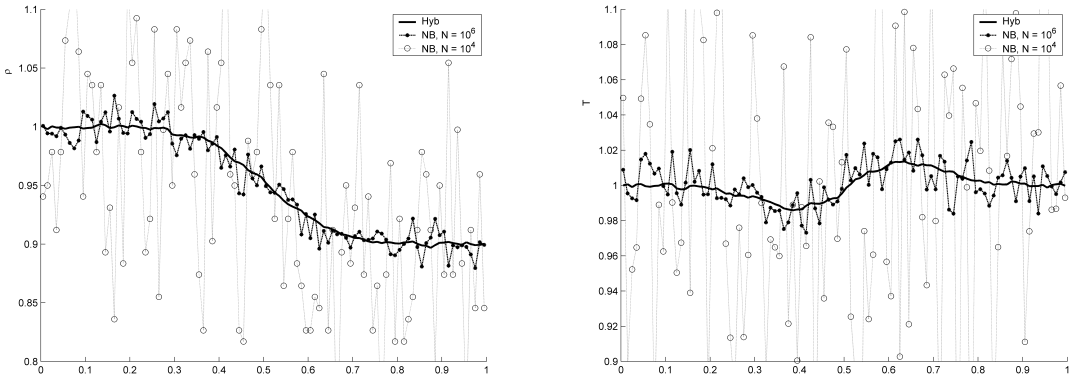

(a) Density profile

(b) Temperature profile

Figure 9: Test case 4, $Kn = 1$, $t = 0.12$. Density and temperature profiles for the NB3 scheme (circles), the NB4 scheme (dotted line), and the hybrid algorithm (continuous line)

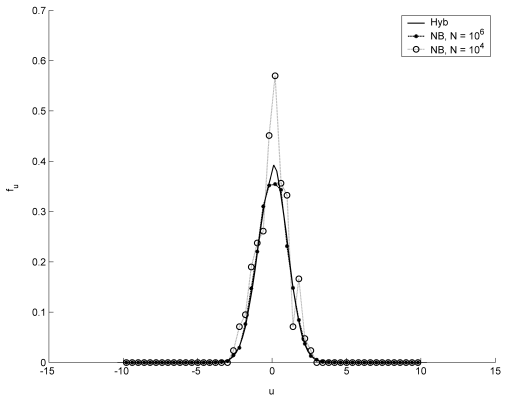

Figure 10: **Test case 4**. Velocity histogram with respect to the first component of the microscopic velocity in $x = 0.5$ at $t = 0.12$ for the NB3 (circles), the NB4 scheme (dotted line), and for the hybrid algorithm (continuous line)

	N	relax.	trans.	overall
NB3 (10^4 particles)	162	0.018	0.035	14.3
NB4 (10^6 particles)	24,144	0.270	3.125	512.3
Hyb	273	1.875	0.172	256.5

Table 7: CPU times [sec.] for test 4

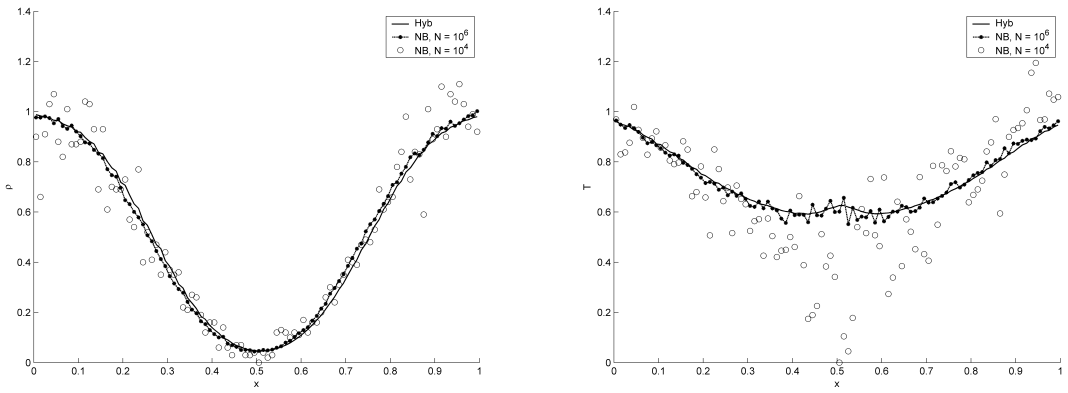

(a) Density profile

(b) Temperature profile

Figure 11: Test case 5, $Kn = 1$, $t = 0.12$. Density and temperature profiles for the NB3 scheme (circles), the NB4 scheme (dotted line), and the hybrid algorithm (continuous line)

	N	relax.	trans.	overall
NB3 (10^4 particles)	142	0.016	0.031	14.1
NB4 (10^6 particles)	18,476	0.235	2.781	442.6
Hyb	218	1.750	0.188	236.7

Table 8: CPU times [sec.] for test 5

6 Conclusions and final remarks

Numerical results presented in the previous section for both space homogeneous and one-dimensional problems show that the hybrid method is able to reproduce the correct relaxation dynamic as in the NB scheme. Moreover stochastic fluctuations obtained on both macroscopic and microscopic levels are strongly reduced using less particles with respect to a DSMC simulation.

However, the hybrid scheme is characterized by an additional cost which comes from the projection step. More specifically, the computational cost of the projection step is proportional to N^2 (where N is the number of particles sampled at the beginning of each relaxation step); thus the computational efficiency of the hybrid algorithm strongly reduces as the ratio ρ_c/ρ approaches 1.

On the contrary, at large Knudsen numbers few particles must be sampled and projected onto the velocity grid and the computational cost of the hybrid scheme is roughly the same as for the DSMC method with approximatively the same number of particles candidate for collision. However the stochastic noise is much smaller than in a DSMC simulation which makes the hybrid algorithm suitable for simulating rarefied flows.

In the second part of the present work, we will employ the hybrid scheme as a Boltzmann solver in a domain decomposition framework, that is we will use the hybrid algorithm to solve the Boltzmann equation in regions where the gas is locally rarefied and far from thermal equilibrium. Some results are anticipated below, for further details we refer the reader to the forthcoming paper [1].

In figs. from 12 to 14 we report numerical results for the test case 3 with a Knudsen number $kn_\infty = 10^{-3}$. Specifically in fig. 12 we report the density profile at two different times $t = 0.6$ (left) and $t = 0.12$ (right), while in figs. from 13 and 14 we report the temperature profile and the indicator used for the domain decomposition at the same times. In figs. from 15 to 17 we report

the same quantities but for a Knudsen number $kn_\infty = 10^{-1}$.

In all figures we use the following convention: a vertical dashed line indicates the interface between two different regions. Euler region (i.e. those region of the computational domain where Euler equations are integrated) are indicated with the letter 'E' at the top of the figure, while BGK and Boltzmann regions are indicated with the letters 'b' and 'B' respectively.

In Euler and BGK regions the Euler equations and the BGK equation are respectively solved using a finite volume scheme, while in Boltzmann regions we employ the hybrid scheme presented in this paper. Numerical results obtained for $kn_\infty = 10^{-1}$ are compared with those provided by the DSMC scheme, while at $kn_\infty = 10^{-3}$ we only report the numerical results provided by the coupled scheme, since the computational time of the DSMC scheme is prohibitive (this is mainly due to the time step restriction on the relaxation step which is proportional to the Knudsen number).

In all cases the domain decomposition varies in time. At $kn_\infty = 10^{-3}$ a kinetic region is correctly detected in the shock layer at the beginning of the simulation (see fig. 12). The BGK model is thus used across the shock since at such a small Knudsen number, the BGK model mimics the dynamic of the Navier-Stokes equations. However it should be stressed that the transport coefficients provided by the BGK model are not correct (for instance the Prandtl number is 1 instead of 2/3). This problem is fixed in [1] where the ES-BGK model is used instead of the BGK equation.

The kinetic region across the shock is still visible at $t = 0.6$, however due to the relaxation processes, the solution relaxes toward the local equilibrium so that at the final time, the whole computational domain is marked as a Euler region with this resolution in space.

At $kn_\infty = 10^{-1}$ and $t = 0.6$, a kinetic region is again detected in the shock layer, however since the the Knudsen number is large the Boltzmann equation is solved instead of the BGK model. On the contrary a small deviation from the local equilibrium is detected in the region across the rarefaction wave and the BGK equation is coherently used. Lastly, before the rarefaction wave and after the shock layer, the gas is still unperturbed thus $f = \mathcal{M}_f$ and consequently Euler equation are used even if the local Knudsen number after the shock layer is large.

At the final time due to the propagation of perturbations on f, most of the domain is marked as a Boltzmann region. Indeed at $kn_\infty = 10^{-1}$ the relaxation time is of the same order than the final integration time, thus at $t = 0.12$ the solution has not still relaxed onto the local equilibrium.

Results obtained for $kn_\infty = 10^{-1}$ are compared with results provided by the NB scheme with 10^4 and 10^6 particles in the whole computational domain (configurations NB3 and NB4). As shown in fig. 15 density profiles are in good agreement. On the contrary some remarkable differences are present in temperature profiles (see fig. 16). Note however that such discrepancies are detected in the BGK region (marked with 'b'). The reason of this difference is due to the incorrect transport coefficients inherent in the BGK equation. In particular the Prandtl number of the 'BGK gas' is 1 instead of the correct values of 2/3 for a monatomic gas. This problem will be fixed in [1] by using the ES-BGK ([17])model instead of the BGK equation, by means of which one is able to recover the correct Prandtl number (see [2]).

Finally in table 9, we report the CPU time required by the coupled hybrid scheme and NB simulations. Note that for a Knudsen number of $kn = 10^{-1}$ the computational time required by the hybrid method is much smaller than the computational time required by the NB4 scheme, and results are affected by stochastic fluctuations whose magnitude is negligible if compared with both density and temperature excursions. On the contrary numerical results provided by the NB scheme even with 10^6 particles present significant stochastic fluctuations.

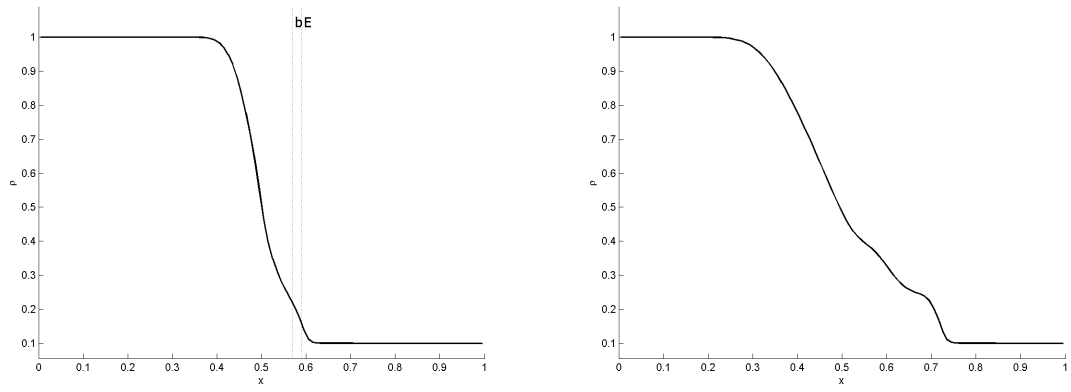

(a) $t = 0.6$ profile

(b) $t = 0.12$ profile

Figure 12: Test case 3, $Kn = 10^{-3}$, Density profile for the coupled scheme at different times

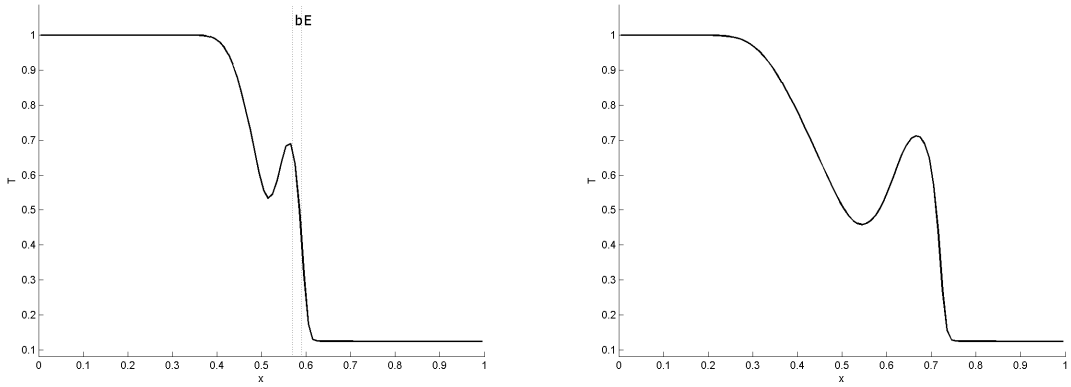

(a) $t = 0.6$ profile

(b) $t = 0.12$ profile

Figure 13: Test case 3, $Kn = 10^{-3}$, Temperature profile for the coupled scheme at different times

	$kn = 10^{-3}$	$kn = 10^{-1}$
NB3	508.4	10.1
NB4	-	1583.4
Coupled	200.1	201.8

Table 9: Comparison between the CPU times [sec.] of the coupled hybrid method and NB scheme for test 3

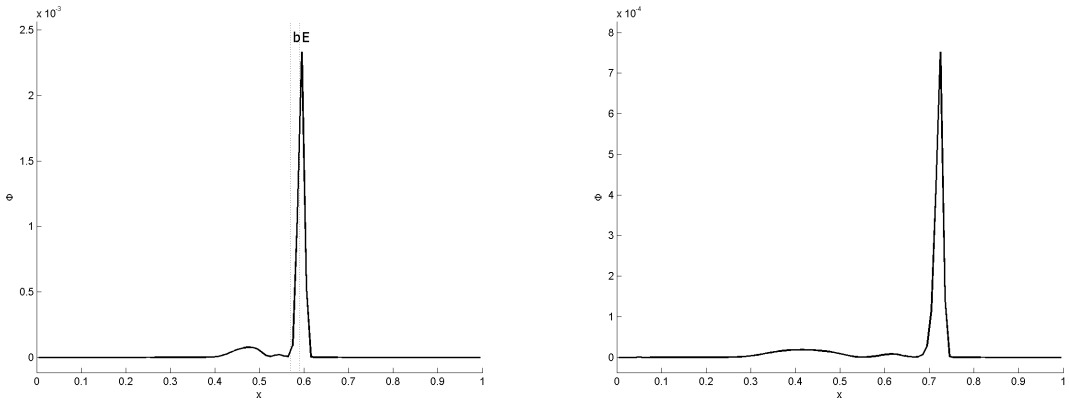

(a) $t = 0.6$ profile (b) $t = 0.12$ profile

Figure 14: Test case 3, $Kn = 10^{-3}$, domain decomposition indicator at different times

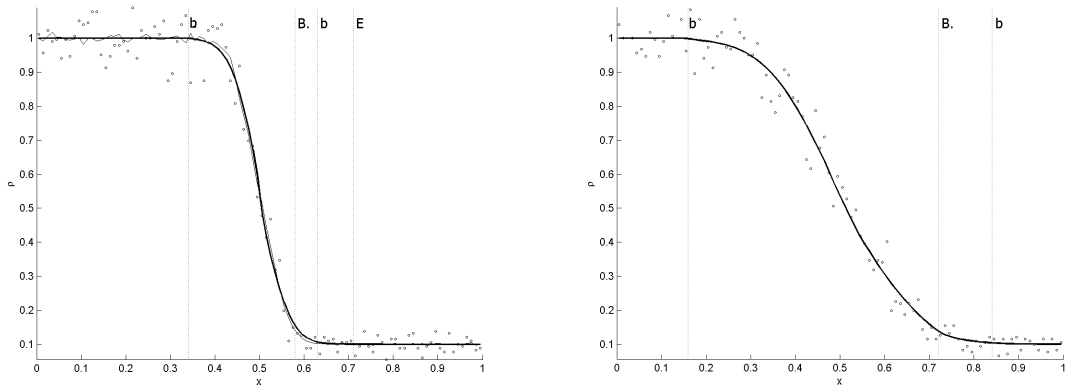

(a) $t = 0.6$ profile (b) $t = 0.12$ profile

Figure 15: Test case 3, $Kn = 10^{-1}$, Density profile for the coupled hybrid scheme (solid line), for NB3 scheme (circles) and for the NB4 scheme (continuous thin line)

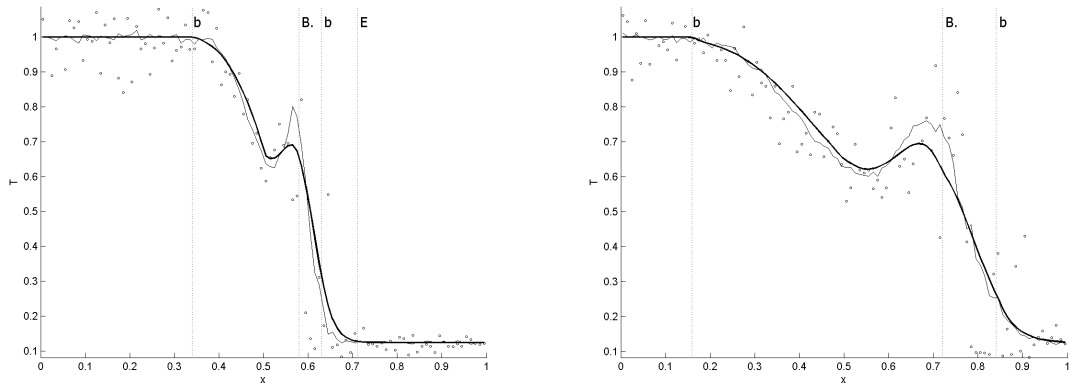

(a) $t = 0.6$ profile

(b) $t = 0.12$ profile

Figure 16: Test case 3, $Kn = 10^{-1}$, Temperature profile for the coupled hybrid scheme (solid line), for NB3 scheme (circles) and for the NB4 scheme (continuous thin line)

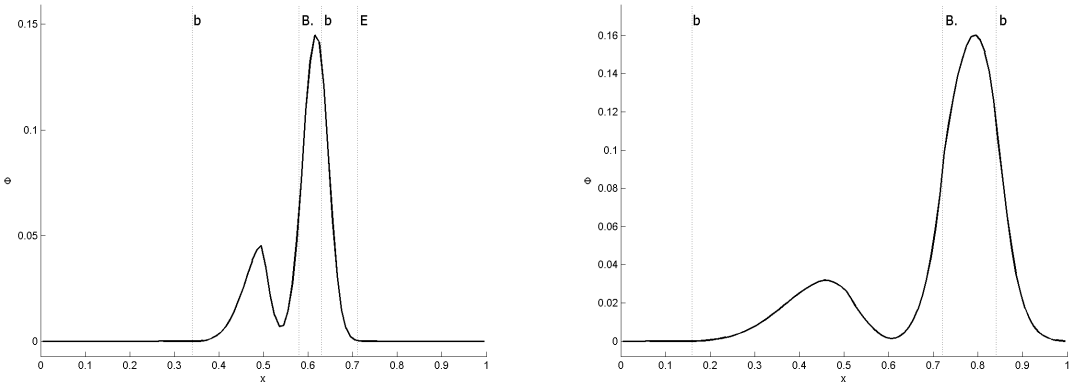

(a) $t = 0.6$ profile

(b) $t = 0.12$ profile

Figure 17: Test case 3, $Kn = 10^{-1}$, domain decomposition indicator at different times

References

[1] Alaia A., Puppo G. *A hybrid method for hydrodynamic-kinetic flow - Part II - Coupling Boltzmann, BGK and Euler equations through domain decomposition strategy*, in preparation.

[2] Andries P., Bourgat J.F., Le Tallec P., Perthame B. *Numerical Comparison between the Boltzmann and ES-BGK Models for Rarefied Gases*, Comput. Methods Appl. Mech. Engrg. 191, (2002)

[3] Babovski, H., *On a simulation scheme for the Boltzmann equation*, Math. Methods Appl. Sci. 8 (1986)

[4] Bhatnagar P.L., Gross E.P., Krook M., *A Model for Collision Processes in gases I. Small Amplitude Processes in Charged and Neutral One-Component Systems*, Phys. Rev. 94 (1954)

[5] Bird G. A., *Molecular Gas Dynamics and the Direct Simulation of Gas Flows*, Oxford University Press (1994)

[6] Bourgat J.F., Le Tallec P., Tidriri M.D. *Coupling Boltzmann and Navier Stokes equations by friction*, Journal of Comput. Physics 127 (1996)

[7] Bourgat J.F., Le Tallec P., Perthame B., Qiu Y. *Coupling Boltzmann and Euler equations without overlapping*, Amer. Math. Soc, (1994)

[8] Caflisch R., Jin S., Russo G., *Uniformly accurate schemes for hyperbolic systems with relaxation*, SIAM, J. Numer. Anal. 34 (1997)

[9] Cercignani C., *The Boltzmann equation and Its Applications*, Springer (1988)

[10] Cercignani C., *Rarefied Gas Dynamics: From Basic Concepts to Actual Calculations*, Cambridge University Press (2000)

[11] Cercignani C., Illner R., Pulvirenti M., *The Mathematical Theory of Dilute Gases*, Springer (1994)

[12] Chapman S., Cowling T.G., *The Mathematical Theory of Non-Uniform Gases*, American Journal of Physics (1962)

[13] Degond P., Jin S., Mieussens L. *A smooth transition model between kinetic and hydrodinamic equations*, Journal of Comput. Physics, 209 (2005)

[14] Dimarco G., Pareschi L., *Hybrid Multiscale Methods I. Hyperbolic Relaxation Problems*, Comm. Math. Sci., vol. 4 (2006)

[15] Dimarco G., Pareschi L., *Hybrid multiscale Methods II. Kinetic Equations*, SIAM J. Multiscale Modeling and Simulation, (submitted)

[16] Garcia A.L., Bell J.B., Crutchfield W.Y., Alder B.J. *Adaptative mesh and algorithm refinement using Direct Simulation Monte Carlo*, Journal of Comput. Physics 154 (1999)

[17] Holway L. H. *Kinetic Theory of Shock Structure using an Ellipsoidal Distribution Function*, Academic Press (1966), pp. 193 - 215

[18] Karniadakis G., Beskok A., Narayan A., *Microflows and nanoflows: fundamentals and simulation*, Springer (2005)

[19] LeVeque R., *Numerical methods for conservation laws*, Birkhauser Verlag (1992)

[20] Mieussens L., *Discrete Velocity Model and Implicit Scheme for the BGK Equation of Rarefied Gas Dynamics*, Models and Methods in Applied Sciences, Vol. 10, No. 8 (2000)

[21] Mieussens L., *Discrete Velocity Models and Numerical Schemes for the Boltzmann-BGK Equation in Plane and Axisymmetric Geometries*, Journal of Comput. Physics 162 (2000)

[22] Nanbu K., *Direct Simulation scheme derived from the Boltzmann equation I. Monocomponent Gases*, J. Phys. Soc. Japan 49 (1980)

[23] Pareschi L., Russo G. *An Introduction to the Numerical Analysis of the Boltzmann Equation*, Riv. Mat. Univ. of Parma (2005)

[24] Pareschi L., Russo G. *Implicit-Explicit Runge-Kutta methods and applications to hyperbolic systems with relaxation*, J. Sci. Comput. 25 (2005)

[25] Perthame B., *An Introduction to Kinetic Schemes for Gas Dynamics*, Lect. Notes Comput. Sci. Eng., Vol. 5, Springer, Berlin (1999)

[26] Perthame B. *Introduction to the theory of random particle methods for Boltzmann equation*, in Advances in Kinetic Theory and Computing, World Sci. (1994)

[27] Pieraccini S., Puppo G. *Implicit -Explicit schemes for BGK kinetic equations*, Journal of Sci. Comput., 32 (2007)

[28] Schwartzentruber T.E., Scalabrin L.C., Boyd I.D., *A modular particle continuum numerical method for hypersonic non-equilibrium gas flows*, J. Comp. Phys., 225, (2007).

[29] Succi S. *The Lattice Boltzmann Equation for FLuid DYnamics and Beyond*, Oxford University Press (2001)

[30] Tcheremissine F. G., *Conservative evaluation of Boltzmann Collision Integral in discrete ordinates approximation*, Computers Math. Applic. 35, pp. 215-221 (1998)

[31] Tiwari S.,*Coupling of the Boltzmann and Euler equations with automatic domain decomposition*, Journal of Comput. Phys. 144 (1998)

[32] Tiwari S., Klar A., *An adaptive domain decomposition procedure for Boltzmann and Euler equations*, J. Comput. Appl. Math. 90 (1998)

[33] Wu J.-S., Lian Y.-Y., Cheng G., Koomullil R.P., Tseng K.-C., *Development and verification of a coupled DSMCNS scheme using unstructured mesh*, J. Comp. Phys., 219, (2006).